DESIGN, SIMULATION, AND CONSTRUCTION OF A SERIES HYBRID ELECTRIC VEHICLE

By:

Daniel Northcott

A Thesis submitted to the Faculty of Graduate Studies of

The University of Manitoba

In partial fulfilment of the requirements for the degree of

MASTER OF SCIENCE

Department of Electrical and Computer Engineering

University of Manitoba

Winnipeg

ABSTRACT

This thesis evaluates a series hybrid electric drivetrain design for use in parking patrol vehicles. Due to the particular attributes of this application, it is proposed that the design would improve the energy efficiency of such a vehicle. The scheme is evaluated in depth through the use of electromagnetic transient simulation tools, which are used to create a highly accurate model of the vehicle. A prototype vehicle of the same design is built, and used to verify and improve the accuracy of the simulation model. The simulation model is then used to predict the energy efficiency of the series hybrid design for parking patrol. This simulation based design strategy is proposed as a method for more rapid and cost effective design of hybrid electric vehicles.

ACKNOWLEDGEMENTS

The author owes a debt of gratitude to the various parties from the University of Manitoba and Westward Industries Ltd., who have worked hard to form a new industrial-academic partnership. Erwin Dirks and Randy Thomas deserve credit for their early work in forming this partnership. Dr. S. Filizadeh has been instrumental the success of this project, with his continual guidance and encouragement throughout. Shane Griffin, Erwin Dirks, and Larry Mauws have also provided solid technical insight and valued feedback. I would also like to thank my friends and family, who have been incredibly supportive throughout this endeavor.

Financial assistance has been provided by Westward Industries Ltd. and the Natural Science and Engineering Research Council (NSERC) through an Industrial Postgraduate Scholarship (IPS).

TABLE OF CONTENTS

LIST OF TABLES

LIST OF FIGURES

1 INTRODUCTION

1.1 Automobiles

Automobiles are an important part of everyday life for many people. The freedom to travel long distances at a reasonable cost is something that society has come to rely on heavily. For the last 100 years or so, automobiles have most often been directly powered by internal combustion engines burning fossil fuels. This particular system is often referred to as 'conventional'. More recently, a great deal of interest has developed around improving the efficiency, reducing the emissions, and reducing the cost of fuel to operate motor vehicles. One possible solution, which is currently gaining acceptance, is to move from conventional vehicles to hybrid vehicles.

1.2 Hybrid Vehicles

In a hybrid vehicle, two or more power sources work together to deliver performance that is greater than for any single source working alone. Through design, it is possible to improve such characteristics as acceleration, emissions, fuel efficiency, and total cost of ownership. Which of these characteristics see the greatest improvement will depend on the design of the system and the control strategy employed.

In a conventional vehicle, the powertrain generally consists of an internal combustion engine and a multi-geared mechanical transmission. The engines in use are normally spark ignition (SI) gasoline powered or compression ignition (CI) diesel powered. As an automotive power plant, the internal combustion engine working alone has proven itself to be quite suitable for many decades. But in recent times, with

declining fuel supplies and the increased environmental awareness of the general public, it is apparent that this strategy is not meeting the needs of society.

In the future, it is predicted by many [1] that fuel cells and/or batteries will replace internal combustion engines completely, but these technologies must improve a great deal before this could occur. Fuel cells are as much as 20 years away from widespread commercial viability, as high costs, poor cold start performance, and hydrogen storage issues all remain to be solved [2]. Batteries are much closer to being a viable replacement on their own, with recharge time, longevity, and cost being the main issues [3]. Because there is no new technology ready to completely usurp engines, the best course of action is to find ways to make better use of them. Hybridizing internal combustion engines with batteries is potentially a viable way to do this.

This thesis will investigate the hybridization of an internal combustion engine with batteries to form a Hybrid Electric Vehicle (HEV) powertrain. The application for this study will be a three-wheeled parking patrol vehicle marketed in the United States called the GO-4. This vehicle is currently offered with a conventional gasoline internal combustion engine. The particular end use of parking patrol has some distinct factors that will affect the design.

1.3 The GO-4

The GO-4 is a small three-wheeled vehicle manufactured by Westward Industries Ltd. This vehicle is classified as a three-wheeled motor cycle in the United States, and is used by parking enforcement agencies in many major US cities. The small, single-occupant vehicle has some operational advantages over small cars, since it allows operators to easily enter and exit from both sides to write citations. Table 1.1 shows some

brief specifications of the currently offered gasoline model. A picture of the vehicle is shown in Figure 1.1.

Table 1.1 - GO-4 gasoline model general specifications

Characteristic	Specification
Engine	1 L 4-cylinder 61 hp spark ignition
Transmission	4 speed automatic
Vehicle Weight	1435 lbs
Size	118“ long, 52.5“ wide, 69.5“ high

Figure 1.1 - The GO-4 gasoline powered parking patrol vehicle

1.4 Motivation

The GO-4 is used as a parking enforcement vehicle in dense urban areas. As such, it is required to drive slowly up and down city streets in a repetitive cycle, stopping every so often to write tickets. This type of usage results in a great deal of idling time, a large amount of wasted fuel, and unnecessary emissions. The possibility of reducing the total lifetime operating costs of these vehicles while reducing their environmental impact through drivetrain hybridization is a sensible goal.

One of the main markets for the GO-4 is in California, where state legislation has been markedly stricter about the amount and type of air emissions from motor vehicles.

Penalties for high emission and incentives for low emission vehicles are part of the law in this particular state. These incentives for low emission vehicles can significantly improve the economics for hybrid electric vehicles.

1.5 Problem Definition

The goal of this work is to design the electric drive portion of a series hybrid drivetrain around a current GO-4 chassis. The topology of this vehicle will be such that it will allow operation in the electric mode, with future provisions to add an engine re-charger, or range-extender unit. The design will use commercially available components whenever possible, along with custom control hardware and software.

The selection of proper components for the drivetrain will be according to requirements of the final use. These requirements will be obtained from the end users, field measurements, and reasonable estimations. The design of the drivetrain will make use of PSCAD/EMTDC electromagnetic transient simulation software in order to verify all requirements are met. This software has found widespread use in the power systems utilities market, especially where power electronics are involved in a design. The software has provided some unique benefits to that particular industry, and it has been selected here in the hopes of bringing the same benefits to this project. Since PSCAD/EMTDC has not been used in this way before, some modification is necessary to model the vehicle effectively.

Finally, a physical prototype of the vehicle is to be built and tested. The results of the simulation will be checked against measurements from the prototype and any major differences reconciled. Once completed, the simulation and prototype together will act as

a basis for an integrated design procedure using simulation and optimization to improve hybrid and electric vehicle designs before prototypes are built.

1.6 Outline of Thesis

Hybrid Electric Vehicles require a meshing of the traditional mechanical components with electric motors, power electronics, and a great deal of digital controls. Chapter 2 will present the high level design theory for HEVs. Alternative topologies for the design of a hybrid powertrain will be introduced and discussed. A brief examination of the strategies used for other hybrid vehicles on the market and future trends will be presented.

Chapter 3 will present the overall design employed for the GO-4 hybrid powertrain. The final design is strongly dependant on the existing technologies and components already available on the market, and so these factors will be discussed. Since this research involves the development of a simulation model and a physical prototype together, it is important that the two are developed in compliance with a single master plan, which is both theoretically and physically realistic.

Chapter 4 will detail the development of a high accuracy electromagnetic transient simulation model for the hybrid vehicle. Methods for modeling the power electronics, motors, controls, and vehicular dynamics are presented.

Chapter 5 will present the prototype of series hybrid drivetrain that has been built. Features of the design and integration of the different required technologies will be discussed.

Chapter 6 will analyze the similarities and differences observed between the simulation case and the constructed prototype, and explore the reasons for these. Methods

and strategies will be presented to improve the accuracy of the simulation model by extracting parameters through physical measurements and empirical calculations. Finally, Chapter 7 will conclude the thesis by presenting the contributions and recommendations for future work.

2 BACKGROUND

2.1 Factors Influencing the Adoption of HEVs

The idea of hybrid vehicles has been around for many years. Significant modern research into hybrid electric vehicles was occurring in the late 1970's in the USA [4] as a reaction to the oil crisis. Since then, there have been many advances in the areas of power electronic devices, microprocessor controls, and battery technology. At the same time, the costs associated with deploying this technology has continuously decreased.

Also of interest lately is the rapid increase in world oil prices. For the most part, this has been due to geopolitical instability and natural disasters, but it has been amplified by the fact the world's oil producers are operating near their maximum production capability. They are not running out of oil, but it is getting more and more expensive to supply. Interest in the environment seems to be growing around the world. Initiatives such as the Kyoto protocol, although not followed by all countries, underscores a general trend toward greater public concern about the environmental impact of greenhouse gasses.

All of these situations taken together; the advancement of technology, rise in energy prices, and growing environmental concern are making hybrid electric vehicles more and more favorable versus conventional vehicles. If hybrids are going to capture major portions of the market, it will be because of the combined advantages over conventional vehicles in all these areas. A significant amount of technological advancement is still required in order to bring hybrid technology from the fringes to the forefront of the automotive marketplace.

In light of these issues, there are several important benefits that hybrid vehicles can provide that conventional vehicles can not:

- Ability to recapture braking energy
- Elimination of engine idling time
- More efficient engine operation and power utilization

These benefits can be used to achieve some or all of the following outcomes:

- Reduced fuel consumption, especially in stop and go driving conditions
- Reduced emissions
- Reduced wear and tear of mechanical components such as the engine, transmission, and brake pads

2.2 Hybrid Topologies

Although the term "hybrid vehicle" has become widely associated with a vehicle using gasoline and electricity for power, the true meaning is actually quite ambiguous. A hybrid vehicle could be built from a combination of any number of power sources of any imaginable kind. Fuel cell hybrids, hydraulic hybrids, and diesel hybrids are a few examples [5] - [7] of this possible diversity. One could also imagine that there is not only a single acceptable way to implement a hybrid with a given set of power sources either. On the contrary, how the hybrid is implemented is just as important as what sources are to be hybridized. In this thesis, only battery electric and gasoline internal combustion engine hybrids will be considered.

There are two common templates used to classify gasoline-electric hybrid vehicle designs: the series hybrid and the parallel hybrid. This is not to say there are only two

ways to design a gasoline-electric hybrid, but that all designs exhibit certain aspects similar to one or both these topologies.

2.2.1 The Series Hybrid Topology

The series hybrid topology is shown in Figure 2.1. The arrows indicate the direction of power flow between components. In this scheme, an electric drive system provides propulsion to the wheels. The electric motors are supplied from energy storage, with the engine and generator recharging this storage as required. The main benefit of this topology is that the gas engine is either entirely off or can run at an optimal operating point (in terms of supplied torque and rotational speed) where it is most efficient [8].

The series topology relies heavily on large energy storage, and requires a high-power electric drive system. The topology is suited to lower speed driving under erratic stop-and-go conditions; an electric drive system can supply torque at low speeds with much higher efficiency than a conventional engine and transmission.

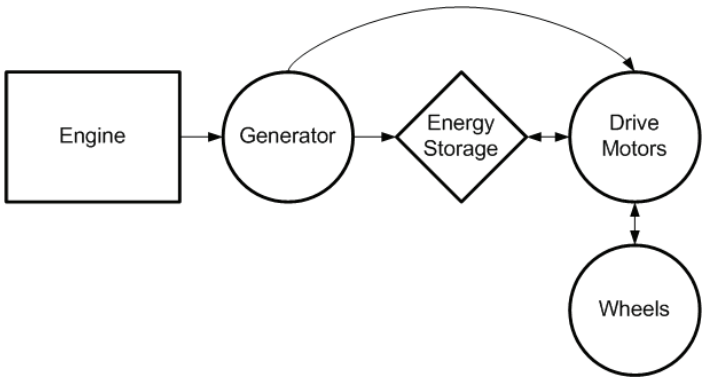

Figure 2.1 - The series hybrid topology

Bidirectional power-electronic converters used for the motor drives allow some of the vehicle's kinetic energy to be recovered during braking. During this time, the drive

motors are operated as generators, and power is returned to the energy storage unit. This is called regenerative braking. In contrast to this, conventional braking systems use friction to dissipate all this kinetic energy as heat.

There are no series hybrids on the market from major automotive manufacturers at the time of this writing. Because the series topology requires a fully sized electrical system which can supply the peak power requirements at full design speed, a great deal of performance is required from the battery bank. In the past, lead acid batteries have been the only affordable solution that could meet the requirements, but are generally too heavy to build such a pack for automotive use. Also, the useful lifetime of these batteries is rather limited. More advanced battery technology, such as Nickel-Metal Hydride or Lithium Ion, could meet the requirements of this series topology but have been prohibitively expensive.

As development continues, Lithium Ion batteries have steadily dropped in price, and energy density has increased to a point where it is reasonable for the automakers to start planning a series hybrid strategy. At the Detroit North American International Auto Show in January 2007, General Motors unveiled the Volt concept car, which is a series hybrid design. This concept marks the first series hybrid design from a major automaker [9]. However the concept car was not actually functional at the time of the show, because an appropriate battery pack was still in the works.

2.2.2 The Parallel Hybrid Topology

The parallel hybrid topology is shown in Figure 2.2. The arrows indicate the direction of power flow between the components. This scheme is characterized by having two or more paths that can deliver mechanical power to the wheels [10]. This topology

sees more diversity in implementation than for the series hybrid, as evidenced by Figure 2.2, where there are many options for the design. Since the propulsion is only assisted by the electric motor(s), the electric system and energy storage can be rated at a lower power than for a series hybrid. This can result in cost, weight, and space savings over a similar performing series hybrid.

At high speeds, such as in highway driving, power can be delivered directly from the engine to the wheels rather than by conversion to and from electricity as in the series hybrid. For lower speed stop-and-go driving, the electrical drive is used more heavily, allowing the engine to be switched off to eliminate wasteful idling. The electrical system can also be used to recapture regenerative braking energy into energy storage, at a rate limited by the electrical power rating, and to a level limited by the state of charge in the storage system.

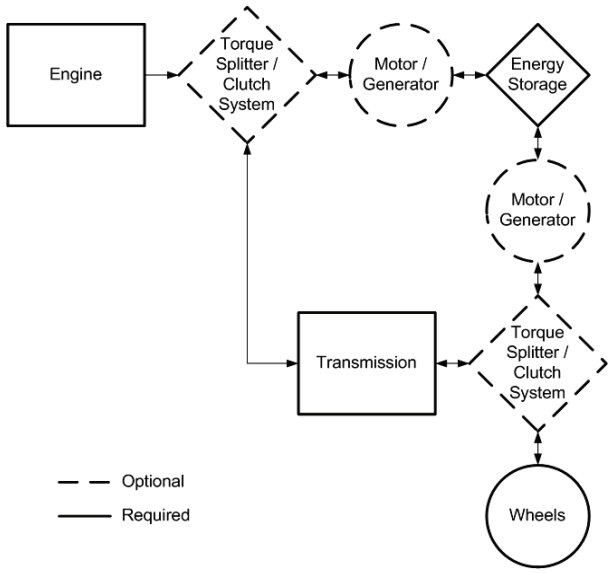

Figure 2.2 - The parallel hybrid topology

Parallel hybrid designs can be very similar to a conventional vehicle drivetrain, which allows an easy transition for vehicle designs. In fact, some hybrid designs are

nothing more than a conventional vehicle with an oversized starter/alternator system. The 2007 Saturn VUE Green Line is a hybrid crossover vehicle for which GM claims a 20% improvement in fuel economy from the standard model [11]. The system also employs some intelligent automatic transmission shift controls in order to capture regenerative braking energy. The electric rating of this design is limited to the torque capability of the rubber belt between the engine and electric machine.

The Ford Escape Hybrid, in contrast, uses a complex gearbox design to allow more flexible operation in all electric, gasoline, and mixed mode operation [12]. The Honda Accord Hybrid uses a design called Integrated Motor Assist (IMA), in which an ac induction motor is inserted between the engine and transmission [13]. This design functions in a similar way to the Saturn VUE Green Line, but uses a higher power electric system and a more rigid mechanical connection. This particular design increases performance of the vehicle as well as the fuel economy.

Toyota Hybrid Synergy Drive (HSD) is a system that combines aspects of parallel and series hybrids [14]. A combination of multiple electric machines, gear boxes, and clutches allows the system to operate in series, parallel, or all-electric mode. The system uses all-electric and series operation at lower speeds, and parallel operation at higher speeds, or when high power is desired, or when the batteries have been depleted. HSD is currently used for all Toyota and Lexus hybrid models.

2.3 Battery Technology

An important factor in the performance, durability, and long term reliability for hybrid vehicles is the energy storage system being utilized. For the purposes of this thesis, ultracapacitors have been excluded from consideration. Table 2.1 lists some of the

more popular competing battery technologies and some expected performance characteristics [16].

Table 2.1 - Expected operating characteristics of competing battery technologies

Battery Type	Energy (Wh/kg)	Power (W/kg)	Cycles (to 80% DOD)	Power / Energy	Energy-Life (#Wh/kg)	Temperature (ºC)
Lead Acid AGM	35	250	400	7	11 200	-30 to 70
NiMH	70	180	1200	2.6	67 200	0 to 40
Lithium Ion	90	220	600	2.4	43 200	0 to 35
Li-polymer	140	300	800	2.1	89 000	0 to 40

Since this thesis is mostly focused on the development of a verified simulation model for the overall hybrid system, less attention will be focused into the area of advanced batteries. In fact, as will be discussed in Chapter 3, cost and market availability present additional important challenges. For these reasons, the batteries will be selected mainly for their simplicity and cost effectiveness of obtaining a working prototype vehicle and a matching simulation. Once such a simulation model has been developed, it is possible to look at other options.

3 DESIGN

3.1 Design Goals

The main goals of this design are to improve the fuel efficiency and reduce tailpipe emissions as compared to the standard gasoline model of the GO-4. By hybridizing a gasoline engine with an electric drive system, it is expected that more efficient usage of the engine while running, and allowing the engine to be turned off at opportune times, will allow these goals to be achieved. Another important issue in the design is the purchase price of the vehicle. If the purchase price is too high in relation to the standard gasoline model, the potential customers will not buy any hybrids.

The drivetrain should also not exceed reasonable volume or weight constraints. It is required that the hybrid drivetrain be compact enough to fit into the standard frame, with some modification. Since the GO-4 is sold as a three-wheeled motorcycle in the US, it is important to stay below the 1500 lb weight restriction. Additionally, since the driving pattern is commonly at a low speed, rolling resistance (which is proportional to weight) is an important loss component for the vehicle. Reducing weight will make the vehicle more efficient, and can allow the use of less expensive and less powerful components.

Finally, it is important that the hybrid vehicle meet performance requirements set by the end users. The operators may be driving slowly for most of their day, but the trip between the work area and home base requires a normal driving speed. The longer this trip becomes, the shorter the productive work day will be for the operator. Since many vehicles are sold to areas with steep roads, such as San Francisco, and it is anticipated that the hybrid would generate strong interest in this market, the drivetrain must be

capable of dealing with the steep and hilly characteristics of the area. A few target specifications for the design are given in Table 3.1.

Table 3.1 - Series hybrid design specifications

Characteristic	Specification
Top Speed	60 km/h
Acceleration (0-40 km/h)	6 s
Hill Climbing Grade	30%
Single Occupant Weight	680 kg or 1500 lbs

To meet these goals for the design, the series hybrid topology is chosen. The series topology is suited well to the unique driving patterns and usage of a parking patrol vehicle. Another factor in the decision is the skills and resources available for this project. Designing a parallel hybrid vehicle suited to this application would require designing an entire mechanical driveline and transmission. The necessary skills and prototyping facilities are not available to the parties involved in the manufacture of the GO-4. It is also nearly impossible to find a manufacturer to build such a system in the small volumes that would be required, for a reasonable price.

3.2 Power Calculations

It is important to analyze the power requirements of a vehicle in the early stages of powertrain design. The results of these calculations are necessary for initially selecting components such as motors, batteries, and power electronic modules for the design. It is very hard to calculate the exact power requirements for the dynamic constraints of the design without performing some type of simulation. So the early calculations are used only as a starting point after which components can be selected and a more detailed analysis can begin.

The first step in finding the required power to drive a road vehicle is to predict the rolling resistance and aerodynamic drag forces, which oppose the motion of the vehicle, and their relationship with vehicle speed. The best way to do this is to perform a coastdown test on the vehicle. During a coastdown test, the vehicle is driven to a reasonably high speed, put into neutral gear if possible, and left to roll unrestricted to a complete stop. A plot of the vehicle speed versus time is recorded during this test. For accurate data, it is best to perform this test on level ground with minimum wind. The condition of the road will also play a factor in the results, and therefore it is common practice to choose a road in good condition with a dry asphalt covering.

A coastdown test was performed by outside parties [18] using a current production model of the gasoline powered GO-4, and the results are shown in Figure 3.1. Also plotted on the graph is a third order polynomial curve of best fit for the data, which is useful for the analysis.

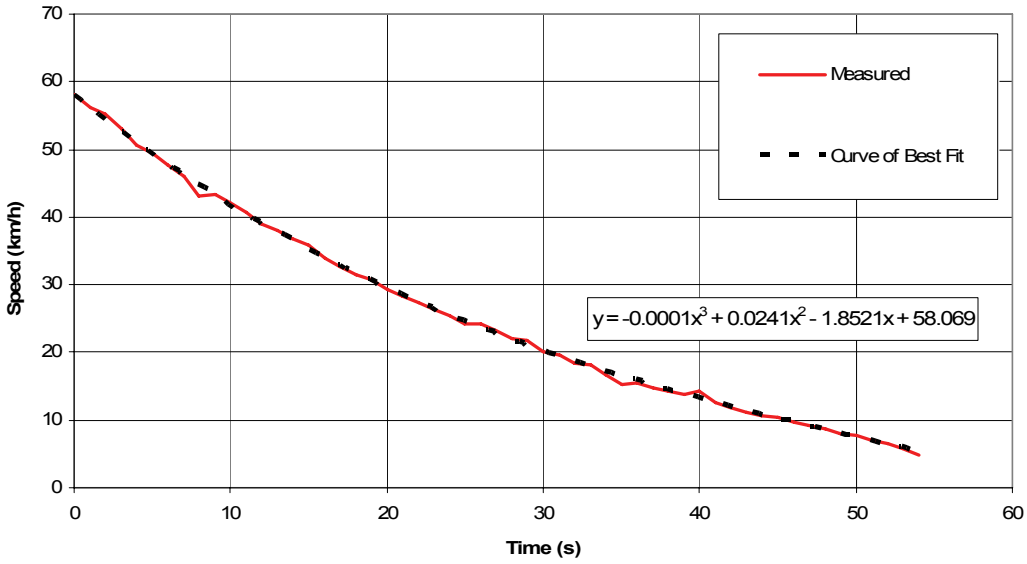

Figure 3.1 - Coastdown test for gasoline powered GO-4 Interceptor II model. (Data used with permission [18])

There exists a simple process to empirically determine rolling resistance and aerodynamic drag coefficients from this data, which can then be used to predict these different forces acting on the vehicle. Once these coefficients are known, it is possible to predict the required power to move the vehicle at any particular speed [19]. The process involves selecting four points on the graph, two at high speed, where aerodynamic and rolling drag are important, and two at low speed, where aerodynamic drag is less significant. These pairs of data points are used to calculate the mean velocities and mean decelerations, which are used in empirical formulas to arrive at the approximate coefficients. Notice there are occasional unsmooth variations in the measured data. This is unavoidable, and is a result of bumps in the road, minor wind gusts, and other such things. Points are taken from the curve of best fit so that the predicted coefficients are not affected. The details of these calculations are given in Table 3.2. A vehicle mass (m) of 680 kg and a frontal cross-sectional area (A) of $1m^2$ are assumed.

Table 3.2 - Empirical calculation of running resistance parameters

Sample Pair 1		**Sample Pair 2**	
t_a, v_a	(0 s, 58.1 km/h)	t_a, v_a	(45 s, 10.37 km/h)
t_b, v_b	(8 s, 43.0 km/h)	t_b, v_b	(52 s, 6.65 km/h)
Mean Velocity: $v_1 = \frac{v_a + v_b}{2}$	50.55 km/h	Mean Velocity: $v_2 = \frac{v_a + v_b}{2}$	8.51 km/h
Mean Deceleration: $a_1 = \frac{v_a - v_b}{t_b - t_a}$	1.89 km/h/s	Mean Deceleration: $a_2 = \frac{v_a - v_b}{t_b - t_a}$	0.53 km/h/s
Aerodynamic Drag Coefficient	$C_d = \frac{6 \cdot m \cdot (a_1 - a_2)}{A \cdot (v_1^2 - v_2^2)} = 2.228$		
Rolling Resistance Coefficient	$\mu = \frac{28.2 \cdot (a_2 \cdot v_1^2 - a_1 \cdot v_2^2)}{10^3 \cdot (v_1^2 - v_2^2)} = 0.0139$		

As mentioned earlier, there are two important opposing forces on a moving vehicle, rolling resistance and aerodynamic drag. These two forces can be predicted by equations 3.1 and 3.2 respectively.

$$F_r = \mu mg \cdot \cos\alpha \tag{3.1}$$

$$F_a = 0.0386 \cdot \rho \cdot C_d \cdot A \cdot (v + v_0)^2 \tag{3.2}$$

In the above equations, F (N) is the force, μ is the rolling resistance coefficient, m (kg) is the mass of the vehicle, g (m/s^2) is the gravitational constant, α is the angle of inclination, ρ (kg/m^2) is the density of air in, C_d is the aerodynamic drag coefficient, A (m^3) is the frontal cross-sectional area of the vehicle, v (km/h) is the velocity of the vehicle, and v_0 (km/h) is the velocity of the headwind. Notice how the cross-sectional area cancels itself out in these equations, and so assuming 1m^2 results in a simplification. These two forces can be translated into power requirements by using equation 3.3 below.

$$P = \frac{v}{3600} F \tag{3.3}$$

Where P_L (kW) is the load power, v (km/h) is the velocity of the vehicle, and F_L is the load force (N) to be converted. By combining all this information, it is possible to generate a graph that predicts the required drive power to maintain a given speed for a vehicle. This is done in Figure 3.2.

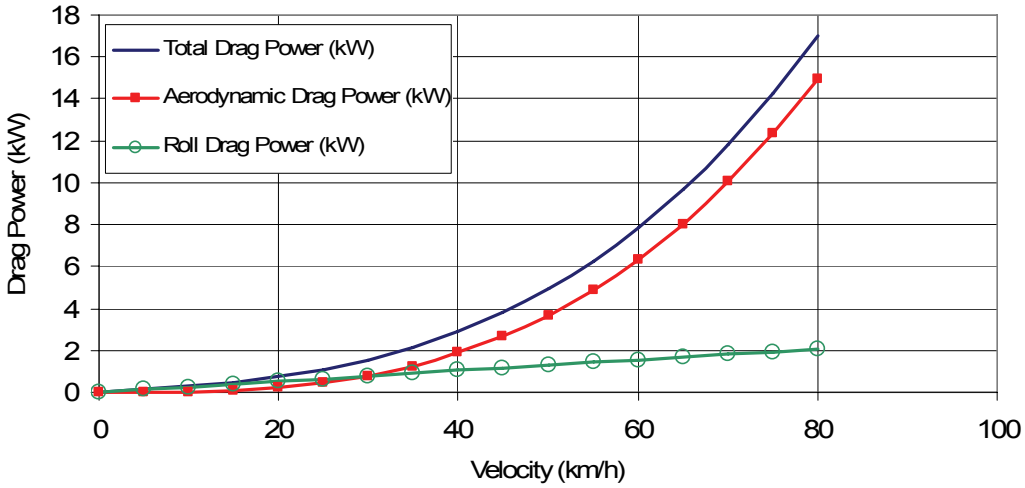

Figure 3.2 - Predicted vehicle rolling and aerodynamic drag losses

Figure 3.2 shows that the static power required to maintain vehicle speed at 60 km/h under ideal conditions would be about 8 kW. Since these calculations are only guidelines for the early stages of design, this figure will be used as a lower bound in component selection. Effort should be made to achieve more than 8 kW to ensure good performance at other speeds, and it is always wise to design for a margin of safety. Figure 3.3 shows the calculated load torque versus speed. This is calculated directly from the power and speed graph in Figure 3.2 using equation 3.4, with r = 0.2794 for the wheel radius. Note that since the zero speed condition produces a 0/0 case, the limit as the speed approaches 0 km/h was taken to calculate the starting torque of 25.907 Nm. This signifies that there is no load torque on a stationary vehicle, but there exists a definite amount of load torque which must be overcome in order to achieve any other speed than zero.

$$T = \frac{3600 \cdot r}{v} P \tag{3.4}$$

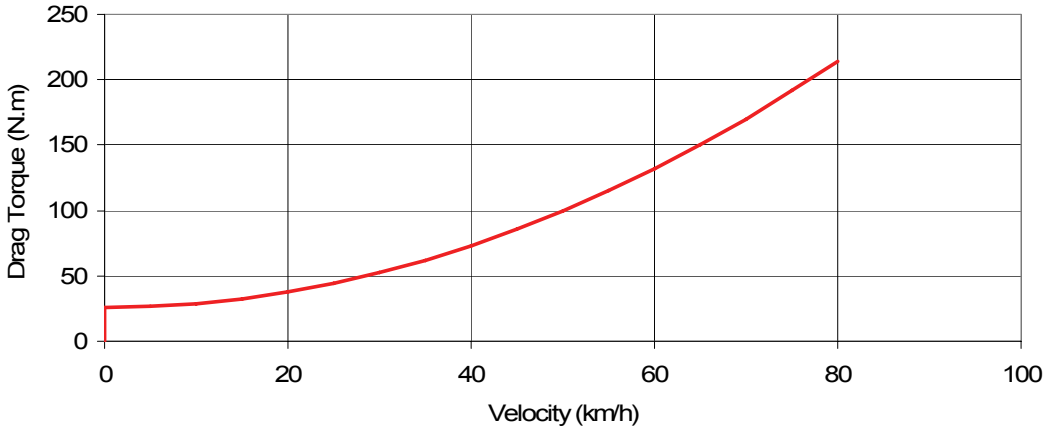

Figure 3.3 - Predicted vehicle load torque versus speed

During this analysis, it was assumed that the hybrid would have similar rolling resistance to the gasoline automatic transmission-equipped vehicle while in neutral. This will likely not be correct, but it should be adequate for first order approximations. Once this process has been followed, a more detailed analysis can be performed by developing an accurate simulation model.

Another important point to consider is how far the vehicle can travel before recharging the battery is necessary, or what is the electric range. With a hybrid vehicle, this is a much less critical calculation than for a pure electric vehicle. The true range of a hybrid vehicle is much more dependant on the size of the gas tank than the size of the battery bank. Graphs like Figure 3.2 should not be used to predict the electric range of a hybrid or electric vehicle based on the Amp-Hour rating of the battery pack. This is because they ignore the power loss due to starting and stopping the vehicle during normal driving, which can be significant, and also ignore the Peukert Effect of the battery, which is an important phenomenon [20]. Power consumption and electric range will be considered in more detail in Chapter 4 where a simulation model is to be developed.

3.3 Commercially Available Components

Since the production volume for the GO-4 is about 500 units per year, it is not worthwhile to do a complete customized design of all hybrid components. This low volume also makes it nearly impossible to convince a supplier to design and produce these types of components exclusively for the GO-4. Therefore it becomes necessary to identify components and devices that are already available on the market that can be accommodated in the hybrid design.

One of the first decisions to be made for the design is the nominal voltage of the system. This will affect the choice of the motors, motor controllers, the design of the battery pack, and the engine re-charger unit. There are several standard voltage levels in common use for golf carts, Neighborhood Electric Vehicles (NEVs), and electric scooters for which there is a considerable amount of these necessary components available. 12V systems are commonly used in automobiles for auxiliary power, but this voltage is much too low for propulsion use because of the high sustained battery currents that would be required. 48V systems are commonly used for golf carts and NEVs, and so this could be a possible choice. 72V systems are used in the high-end golf carts and NEVs, and there exists a considerable market for people seeking to convert a 48V electric vehicle to 72V, meaning that all the necessary components in these two voltage ratings are available commercially.

Higher voltages, such as 96V and 144V are used for some specialty motors, but no commonly available motor drive or 12V auxiliary power DC/DC converters could be found at these voltage ranges. This implies that although there could be some benefits at higher voltages, it would require a great deal of customized power electronics design to

produce a commercial vehicle at these voltage levels. Additionally, it is worthwhile to note the higher the voltage in a system, the longer the string of cells required, and the bigger the chance of cell imbalances, which could cause major problems. There are also reliability and liability issues that could come with so much in-house design work. Therefore, the voltage level of choice for this design is set to 72V.

3.3.1 PERM 72V, 7.2kW Permanent Magnet DC Motor

PERM, a German electric motor company, manufactures these 72V, 7.2kW Permanent Magnet dc motors, which can withstand double the power output (14.4kW) for 10 seconds. Their compact and light design, along with their simple control requirements makes them an excellent choice for the hybrid. The nominal rated speed is 3600 rpm. The motor is shown in Figure 3.4. Compared to AC and other DC motor types, the PMDC machine is much more compact and lighter. It was not possible to find any AC machines and drives for a 72V system, and wound stator DC machines are much harder to implement forward and reverse with regenerative braking.

Figure 3.4 - PERM 72V 7.2kW PMDC motor

3.3.2 DMC 80V 350A PMDC Motor Drive

DMC, also from Germany, designs and sells a family of advanced technology low voltage dc fed motor drives. Each of the available models is designed with a flat structure as shown in Figure 3.5. The drives are built using Insulated Metal Substrate (IMS) technology, which allows the same mass production abilities used to make printed circuit boards for power electronics, using surface mounted IGBTs and MOSFETs. The dc motor drive selected is a four-quadrant IGBT design that allows forward and reverse as well as regenerative braking in both directions. The drives share a CAN-based communication protocol to allow sharing of fault codes and control variables with an LCD display.

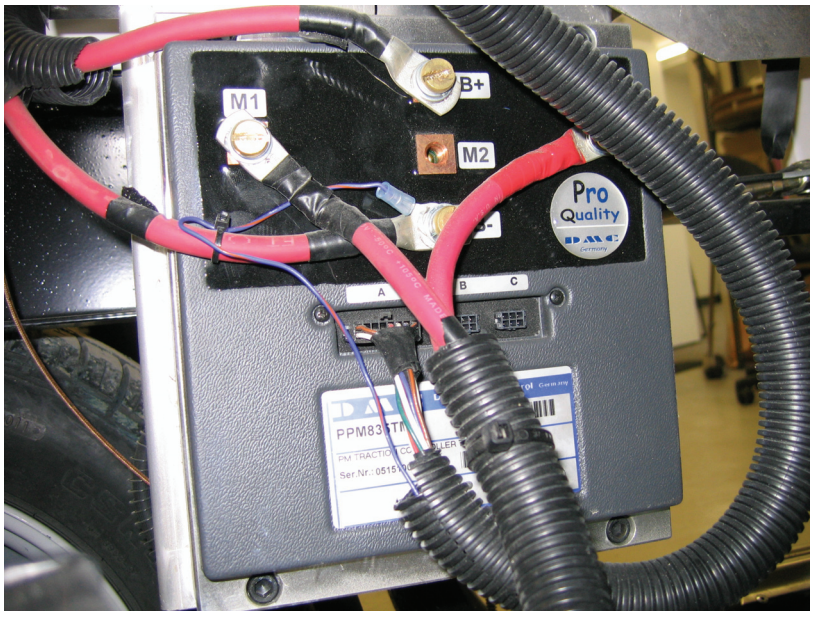

Figure 3.5 - DMC 80V, 350A PMDC motor drive

3.3.3 DMC 72V to 12V DC 300W Isolated DC/DC Converter

Since it is desired to sell this vehicle as street-legal in the United States, it is necessary to meet US Federal Motor Vehicle Safety Standards (FMVSS) in the design.

An important rule for electric and hybrid vehicles in this voltage class is the requirement to keep the main battery pack isolated from the frame [15]. Since most automotive electrical components use the frame as a reference, an isolated power supply must be used if the main battery pack is to supply this 12V system. The alternative is to include a completely different charging system for a dedicated 12V battery, adding more cost, weight, and complication. The converter, shown in Figure 3.6, is encased in protective plastic potting to prevent against environmental damage.

Figure 3.6 - DMC 72V to 12V 300W DC/DC converter

3.3.4 Optima D35 12V, 48Ah Batteries

Energy storage is a very crucial and expensive component of a hybrid electric vehicle. Whether ultracapacitors or batteries are used, it is important to ensure cost is minimized while guaranteeing acceptable performance and lifetime. For this design, it was decided to avoid making these tough decisions and to select lower cost batteries for the purpose of prototyping only. Optima D35 batteries are sealed deep cycle lead acid

Absorbed Glass Mat (AGM) batteries. They are similar in physical dimensions to the Starting, Lighting, and Ignition (SLI) batteries found in most vehicles today. In fact, these batteries are used commonly in utility vehicles where extra capacity is required for high powered lighting. The fact that there is already a high volume market for these batteries makes for cheaper per unit cost regardless of volume to be purchased.

The battery market is currently in a state of flux. A high and sustained amount of research and development money being spent around the globe is resulting in continual technological breakthroughs in battery technology. Portable electronics is a key area that has driven this situation over the last many years, since each of these incremental improvements can lead to greater convenience and acceptance of these devices, without pushing the total cost of the devices out of reach. In effect, there has been a payback for this type of research in the portable electronics industry for some time, but more recently, the automotive industry is beginning to recognize the new potential for these advanced batteries in electric and hybrid vehicles. The result of this is a new critical mass of interest, from multiple industries, is being reached in the research and development area of advanced battery technologies. Much of this interest is focused on the lithium ion battery, and derivatives thereof.

Because of this rapidly evolving situation, the decision was made not to commit to an agreement with a particular lithium ion manufacturer until the vehicle is close to being ready for commercialization. This will ensure the most suitable battery technology at the lowest cost will be delivered with the first commercial units. It is also worth noting that the cheapest lithium ion pack is about seven times more expensive than the Optima D35 pack at the time of this writing. This means, all else being equal, replacing the

Optima batteries every 2 years is cheaper than the lithium ion option over a standard 10 year lifetime of the GO-4. A main consideration in favor of lithium ion is the weight reduction; its effect on vehicle efficiency as well as toward meeting the maximum vehicle weight restrictions for the three-wheeled vehicle class. All of this is impossible to be sure about before the rest of the vehicle has been developed, further reinforcing the strategy of waiting until later in the development.

The Optima D35's are connected electrically in a series string of 6 batteries in order to build up the required 72V. Figure 3.7 shows a picture of the Optima D35, and Table 3.3 gives some general specifications of the resulting 72V, 48Ah battery pack.

Figure 3.7 - Optima D35 12V, 48Ah battery

Table 3.3 - 72V, 48Ah VRLA AGM battery pack specifications

Characteristic	Specification
Nominal Voltage	72 V
Voltage Range	63 V to 78.6 V
Capacity	48Ah on C/20 rate
Weight	99.6 kg
Quick Charge to 90% Capacity	100 A for 35 minutes
Max Current at 0°C for 30 s	810 A

The capacity of these batteries should provide only short duration all-electric range suitable for obtaining the necessary experimental data for verifying the simulation model. This information will then be used in Chapter 6 to study the necessary energy and power required.

3.3.5 Engine and Generator Considerations

For the series hybrid topology, the engine and generator are what distinguish a hybrid vehicle from an electric vehicle. As mentioned earlier, this work is focused primarily on the development of the electrical systems of the hybrid, leaving the engine and generator to be added later. However, it is necessary to have a plan in mind for the inclusion of the generator to the system in an orderly fashion. It is also important to understand some general theory behind gasoline engines so that the design will allow it to be used effectively.

Gasoline Spark Ignition (SI) Internal Combustion Engines (ICEs) use the energy released from igniting an air and fuel mixture to produce power in the form of a rotating shaft. The proper mixture of air and fuel is used to keep emissions low and efficiency high. There are many forms of energy conversion that must take place in a short time for this energy conversion operation to be successful. Firstly, the exploding gasses generate a great deal of heat in a small confined volume within the cylinder, which in turn raises the

pressure in that space. This pressure energy is translated into linear motion as the piston drops, and the volume in the combustion chamber increases. Finally, linear motion is translated into rotational motion by a crankshaft.

The amount of power generated by the engine is controlled by the total amount of fuel and air mixture that is being burned with each of these explosions. Also, the rotational speed of the crankshaft imposes many conditions on how and when each of these energy conversions will take place, and how efficient this conversion will be. Therefore, the operation of an engine is strongly dependant on the amount of fuel input (or power output) and the speed of rotation of the engine. This is a very simplified view of how SI ICEs work, but it is enough to illustrate an important point about their efficient operation. The efficiency of an engine is highly affected by the amount of power being generated and the speed at which the crankshaft is rotating. In the literature [16]-[17], torque and speed are often used to map the efficiency of an ICE. An example of such an efficiency map is shown in Figure 3.8.

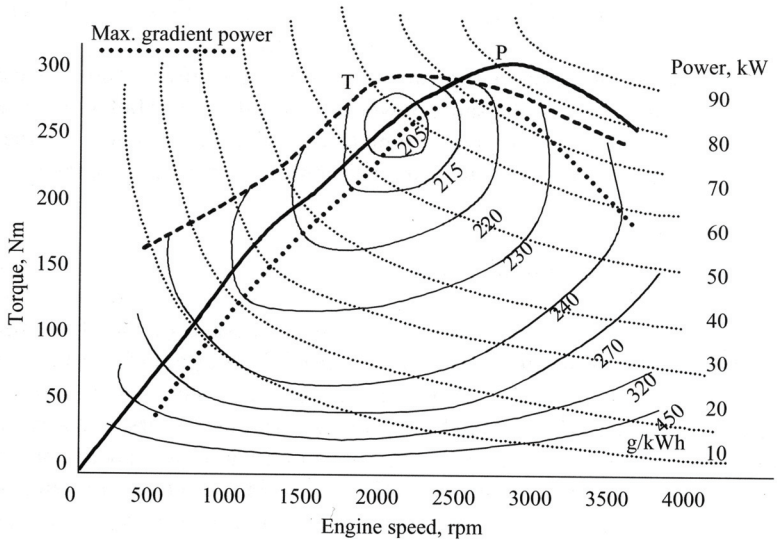

Figure 3.8 - Example engine efficiency map in the torque-speed plane
[Figure used with permission [16]]

Figure 3.8 shows there are loci of constant fuel consumption (measured in g/kWh) in the Torque-Speed plane. The maximum gradient power indicates the most efficient operating point for a given engine speed, and is represented as a dotted line. For a series hybrid vehicle, it is possible to completely decouple an engine from the wheels of a vehicle in terms of power and rotational speed. Therefore is possible to sustain operation at the optimal efficiency point, which corresponds to the lowest grams of fuel per kWh. For the parallel architecture, often the engine speed is still tied to the wheel speed, and only the power output is adjustable by adding or subtracting via the electric machine. In this case, the strategy should seek to keep the engine operation point as close as possible to the gradient line above. However, the rating of the machine and the state of charge of the batteries will limit the effectiveness and length of time this scheme can be employed before the vehicle must resort back to conventional operation.

With this in mind, and because the series hybrid topology has been chosen, it is possible to ignore the engine and generator unit temporarily in order to focus on the electric drive system. At this stage in the design process, it is worthwhile to list a few early stage design goals to be used in the future when an engine is to be integrated. Table 3.3 from the battery section indicates the battery pack is capable of being charged at 100A for 35 minutes to arrive at a 90% state of charge. Of course there are certain conditions on this that must be monitored such as maximum cell voltage and temperature limits that must not be exceeded in the process, which will need to be considered. However, since the recharging operation will take place while the vehicle is driving, and consuming electric power, not all of this current will be flowing into the batteries at all

times. Therefore it is decided that nominal ratings of 100A at 72V would be reasonable for the generator.

Coincidentally, this is exactly the rating of the PMDC machines used for the drive motors. As a side effect, utilizing this machine in three places on each vehicle will increase the volume of machines being purchased from the vendor at one time, which will lead to better cost discounts in the long run. The task remains to find a suitable engine that has its highest efficiency point near 3600 rpm and 7.2kW. If the rpm specification is not convenient, a gear or belt reduction could be used between the engine and generator. A number of engines have been looked at but this would be best decided by a mechanical engineer, and so a selection is not made as part of this work. Table 3.4 lists some approximate specifications.

Table 3.4 - Approximate specifications for engine and generator unit

Characteristic	Specification
DC Nominal Rating	72 V, 100 A
Desired Efficiency Point	7.2 kW at 3600 rpm
Fuel Delivery	EFI preferred

3.4 GO-4 Hybrid Electric Drivetrain

After considering all these initial constraints on the design of the hybrid, brought forward by the numerous limitations from the available commercial components, it is possible to come up with a specific framework for the vehicle design. The overall layout is shown in Figure 3.9. The Engine/Generator has been drawn off-board for clarity in the figure, and also because the design will allow for omission of this component if a pure electric drivetrain is desired in the future. This design is the basis for the co-development

of the simulation model and the prototype vehicle, which are explained in Chapters 4 and 5 respectively.

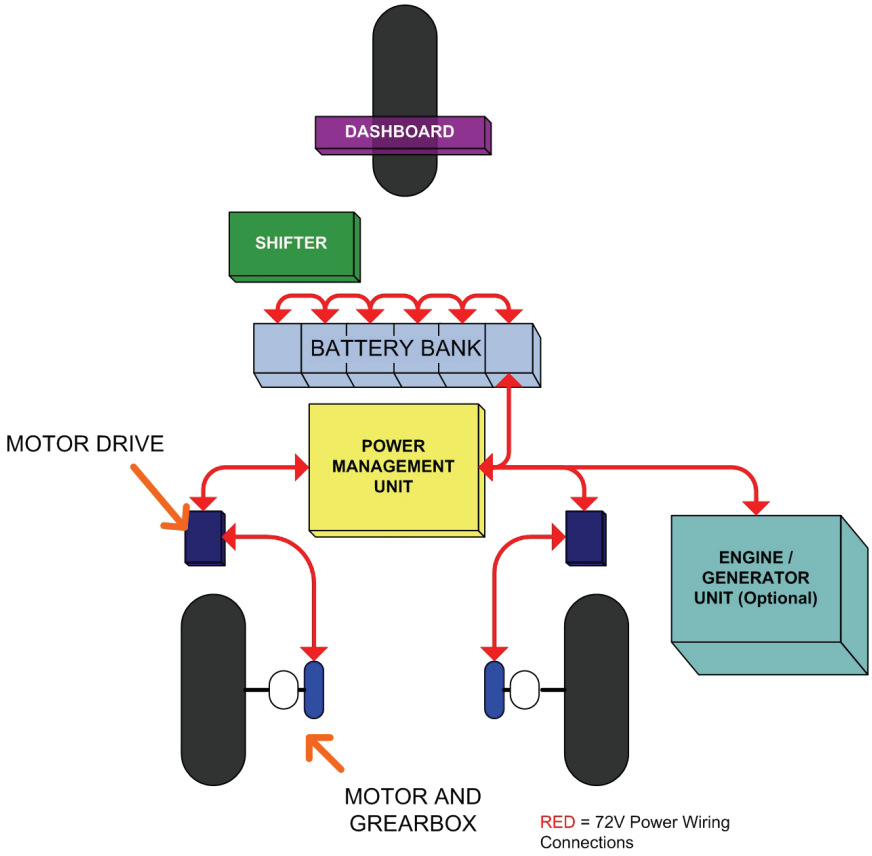

Figure 3.9 - Overall framework for the series hybrid design

4 DEVELOPMENT OF A SIMULATION MODEL

4.1 The Role of Simulation in Design

Since the design of this hybrid electric vehicle is highly constrained by the available commercial components, it is important to identify these components early on in the development stages. It is also important to perform first-order design calculations with the available manufacturer-supplied information. The results of these calculations should be used to provide some insight into the acceptability of the design from the outset, and can indicate the need to make changes to the component selections or to relax design specifications. After this process is done however, there still remains a fair amount of uncertainty regarding the acceptability of the design, and the capability of the selected components, and how they will react together as a system.

By using suitable computer simulation tools, it is possible to determine, with a high degree of certainty, whether the required objectives can be achieved under the current design. If these objectives cannot be achieved with the current design, then it is also possible to evaluate various modifications and alternative courses of action, with the same high level of certainty. This process of simulation is more costly and time consuming than the first round of calculations, but is far more powerful, flexible, and cost effective than to follow the same process by building multiple physical prototypes. The detail that can be captured through simulation is limited only by the available theory, and the time and effort that are put into the development of such models.

This chapter will focus strongly on the development of an accurate simulation model of the electrical drive system. Because the final drive system is purely electrical, a

good quality prediction of the vehicle performance can be gained through this primary focus. The hybrid will have a significantly large electrical storage capacity, and this translates into a significant amount of electric-only driving distance. During this time of electric-only operation, the simulation model will be a good predictor of the vehicle in practice. As for the periods of time when the engine is running, little is known, because this is outside the scope of this thesis. Therefore it is important to provide good electrical energy requirements as a product of this analysis, which can later be used for designing the engine and generator system.

The design process used here aims to take great advantage of computer simulation to reduce the costs and time requirements of prototyping the vehicle, and to provide a long lasting tool that will be useful in the design of future hybrid vehicles.

4.2 Modeling Individual Components of the System

Since a strong focus is being placed on the electrical portion of the drivetrain, it makes sense to use a simulation package for modeling electrical machines and devices, which also has capabilities for modeling the mechanical systems and controls. As discussed in Chapter 1, PSCAD/EMTDC has been chosen as the simulation software for this development. PSCAD has many built-in electrical models and capabilities that will facilitate the development of this model, and these will be used wherever possible. The following sections will detail the modeling procedure used for each component or module in the system.

4.2.1 Motor Simulation Model

As mentioned in Chapter 3, the vehicle will use two 7.2kW, 72V PMDC motors to drive the two rear wheels separately. The dc motor model provided by PSCAD as part of the master library has been used for this purpose. The graphical representation within PSCAD is shown in Figure 4.1.

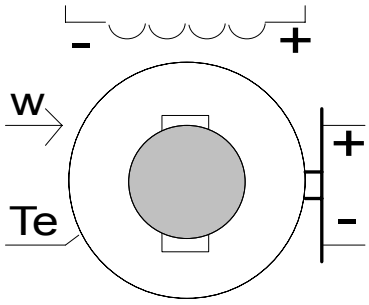

Figure 4.1 - PSCAD dc machine model

The dc machine model is a 4 electrical-terminal device, which includes an armature (right side) and a field circuit (top side). Additionally there is an interface to the per-unit rotational speed, ω (as an input), and the per-unit torque, *Te* (as an output). A PMDC machine has no field circuit, since a magnetic field is naturally produced by the permanent magnets on the stator of the machine. An easy way to deal with this is to enforce a field current to the model that will allow it to function in the same way as the permanent magnet machine. To properly achieve this, it is important to know about the mathematical equations used for the PSCAD model. These are given in equations 4.1 to 4.4.

$$V_f = I_f R_f + L_f \frac{dI_f}{dt} \tag{4.1}$$

$$V_t = E + I_a R_a + L_a \frac{dI_a}{dt} \tag{4.2}$$

$$T_e = k\phi I_a \tag{4.3}$$

$$E = k\phi\omega \tag{4.4}$$

Where V_f is the field voltage, I_f the field current, R_f the field resistance, L_f the field inductance, V_t the armature terminal voltage, E the armature back-emf, I_a the armature current, R_a the armature resistance, L_a the armature inductance, T_e the electrical torque, ω the rotational speed, ϕ the flux in the machine, and k is a constant. It is important to note also that the machine flux is a function of the field current, but since this relationship is non-linear in practice, the model accepts a point-wise linear or exponential curve as an input. Since the flux of the machine is difficult to measure in a laboratory, the input characteristic that is used is the back-emf E versus I_f, at any particular rotational speed ω. Knowing this information, it is straightforward to modify this model to work for a PMDC machine.

In order to deal with the field circuit, a constant current source of 1A was used. Once this is done, the values of the field resistance and field inductance used are not important to this model. Next, it is important to fix the open-circuit voltage versus field current characteristic. Since the field current is now constant, only one point on this curve is important, that corresponding to 1A. By using the information from the supplier of this motor [21], it is a simple task to calculate this.

Table 4.1 - Distributor supplied technical data for PERM PMG132

Parameter	Value
Resistance (Ra)	0.041 Ω
Inductance (La)	0.019 µH
No load angular velocity	3590 rpm
No load current	6 A
Angular velocity constant	50.2 rpm/V

$$E = 72\,\mathrm{V} - 6\,\mathrm{A} \times 0.041\,\Omega = 71.90\,\mathrm{V} \tag{4.5}$$

$$E_{pu}\,(\text{at rated speed}) = \frac{71.90\ \text{V}}{3590\ \text{rpm}} \times \frac{3600}{72} = 1.00\,\text{pu} \tag{4.6}$$

Notice that equation 4.5 is simply equation 4.2 evaluated under steady state conditions. It is also possible to use the angular velocity constant from Table 4.1 as follows:

$$E_{pu}\,(\text{at rated speed}) = \frac{1}{50.2\,\frac{\text{rpm}}{\text{V}}} \times \frac{3600}{72} = 1.00\,\text{pu} \tag{4.7}$$

All that remains is to enter a series of data points for the (*I*, *V*) characteristic that will guarantee a linear slope of 1. Armature reaction was ignored for this model, as the process required to model it is complicated, and the effects on predicted vehicle performance should not be significant. This is a secondary effect and the prototype results (see Chapter 6) will confirm that it has insignificant impact on the modeling stage. The remaining parameters that are needed for the model are taken from the datasheet, which are also available in Table 4.1. The motor is not functional without the connections for T_e and ω. It is also important to consider the fact that *Te*, the electrical torque, is not the same as the mechanical torque that can be seen at the real-life motor shaft. This is because of various windage and friction forces inside the machine. This can be modeled in PSCAD by interfacing the T_e and ω to a mechanical shaft/load model. It is possible to do this by using a library component called the "Multi-Mass Torsional Shaft Interface", but a more relevant vehicular load model will be developed in section 4.2.3.

4.2.2 Motor Drive Simulation Model

The motor drives that have been selected in Chapter 3 are four-quadrant controlled, H-bridge IGBT drives. The four-quadrant control scheme allows the electric

machine to be operated in forward or reverse, as a motor or a generator, all by altering the mode in which the switches in the H-bridge are controlled. A schematic diagram of the H-bridge is shown in Figure 4.2, and a map of the four quadrants of operation in the voltage-current plane is shown in Figure 4.3.

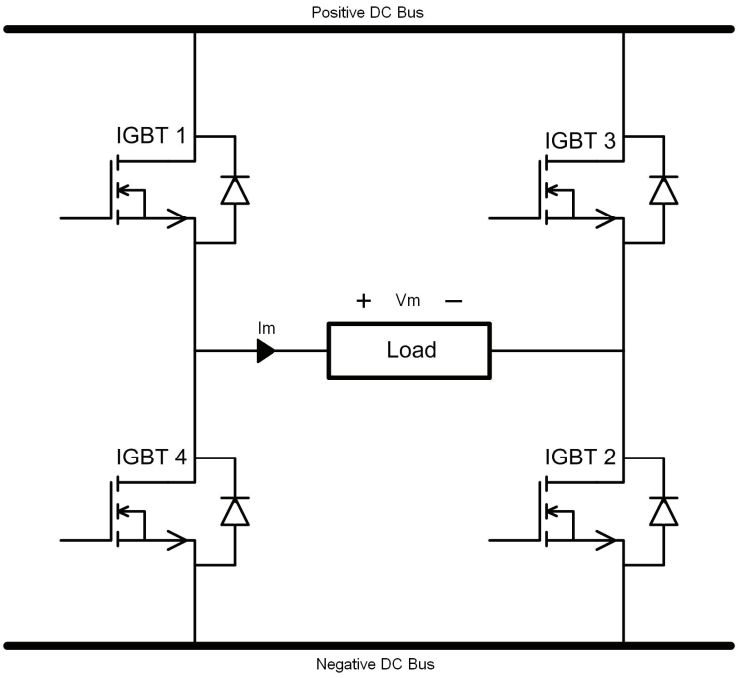

Figure 4.2 - H-bridge IGBT four quadrant drive schematic

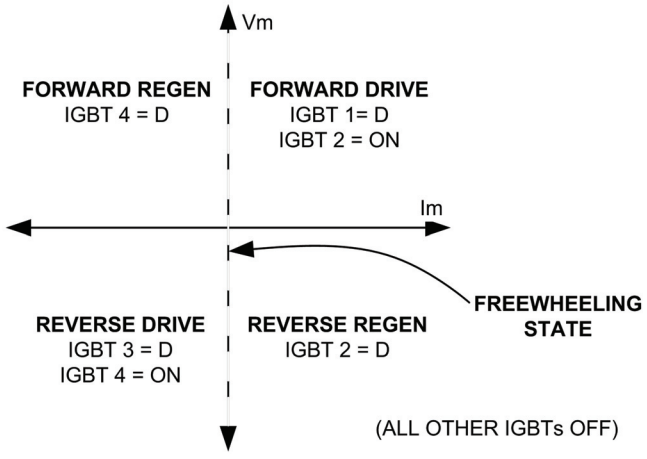

Figure 4.3 - Map of the four quadrants of operation in the voltage-current plane

In Figure 4.3, the IGBT states are given depending on the particular operating point in the voltage-current plane. In this case, the motor voltage V_m is more correctly stated as the open circuit terminal voltage V_t, or the back-emf voltage E. Note that the y-axis corresponds to zero current, and is known as the freewheeling state. Where an IGBT state is given as D, this indicates that a controlled duty cycle is applied to this switch in order to control the motor current. Therefore, to control a permanent magnet electric machine using this type of drive, it is important to determine which state the drive is to be controlled in, and then to apply the control signals to the correct IGBTs.

For this hybrid vehicle, torque control will be used to drive the machines. If speed control were used for this application, when the driver ceases to press the accelerator pedal, theoretically the vehicle would come to an abrupt and violent stop. Therefore, it is most straightforward to use the armature current as the control variable to drive the machines, which is largely proportional to torque. A PI controller will adjust the duty cycle D to arrive at the requested armature current. According to Figure 4.3, the control scheme must first use V_m to determine which IGBTs will be on, and which will receive the duty cycle.

In practice, it is not a straightforward procedure to measure V_m, since while the duty cycled IGBT is turned on, the terminal voltage will be equal to the DC bus voltage. When the duty cycled IGBT is off, the terminal voltage may or may not return to the steady-state open circuit voltage in time, as the inductance and the freewheeling diodes can play a role. By using a model-based procedure, it is possible to predict V_m by using 4.8. However for this simulation it is much easier to use the angular speed to predict V_m.

$$V_t = V_m - i_a R_a - L_a \frac{di_a}{dt} \tag{4.8}$$

There are some cases where it is desired to deviate from this control scheme. For example, when the vehicle is starting from a hill, it may roll back slightly before the driver can apply the accelerator pedal enough. Because it is impossible to extract enough power from a slowly rolling vehicle to stop it, this would be a serious problem indeed. Therefore, it is desired to provide a low-speed margin in which forward drive control is still applied while rolling backward, and vice versa. This is termed the Regenerative Threshold. Beyond this speed, it is anticipated that the driver would choose to use the brakes, although this is not entirely necessary, since regenerative braking in the proper direction will happen naturally via the control scheme in these cases.

Another important consideration that must be made when designing a vehicle with regenerative braking is how to blend this with the conventional mechanical friction brakes. For the purposes of this simulation, it will be of interest to use the regenerative braking system to full advantage, to see how much improvement it can bring. Later, when an actual system is designed, it can be modeled in the simulation and verified. In order to make maximum use of the regenerative braking, it is necessary to allow the drive system to have the first opportunity to apply braking torque, and then supplement this as needed using the mechanical brakes. In order to facilitate this, the drive system will have control of the mechanical braking in the simulation model.

Figure 4.4 shows a custom control block that has been developed in PSCAD to provide the state determination, duty cycle generation, regenerative threshold, and mechanical braking calculations.

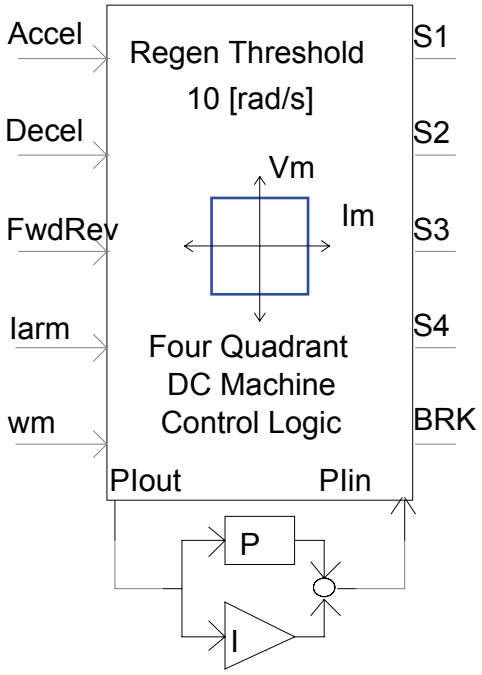

Figure 4.4 - PMDC Machine four-quadrant control system

This control system uses the driver input accelerator and decelerator positions, and the forward/reverse selector along with the vehicle speed to determine the proper delivery of the IGBT gate signals. The armature current reference is determined by subtracting the Decel input from Accel, and applying the appropriate sign. Both the PI input and output can be positive or negative, which allows a smooth transition between accelerating and braking. This armature current reference, which is approximately equivalent to a torque reference, is given to the PI controller through the terminal PIout. The PI controller performs the normal control functions, and returns a duty cycle to the terminal PIin. This duty cycle is delivered to the appropriate switch (S1 – S4) by the logic in the control block.

A summary of the logic employed in this block is given in Table 4.2. $k\varphi$ is a constant used to determine how many Newton-meters of mechanical braking torque to

apply per deficient regenerative amp. S1, S2, S3, and S4 are the IGBT duty cycles for IGBT 1 – 4 respectively, where a value of 1 is always on and 0 is always off.

Table 4.2 - Summary of four-quadrant control logic

State of Operation	Conditions	Outputs
Forward Drive	Accel – Decel > 0 & Forward Selected	PIout = Accel – Decel – Iarm BRK = 0 S1 = PIin S2 = 1 S3 = 0 S4 = 0
Reverse Drive	Accel – Decel > 0 & Reverse Selected	PIout = Accel – Decel + Iarm BRK = 0 S1 = 0 S2 = 0 S3 = PIin S4 = 1
Reverse Regenerative Braking	Accel – Decel < 0 & w < – Regen Threshold	PIout = Accel – Decel + Iarm BRK = – | Accel – Decel – Iarm | * kφ S1 = 0 S2 = – PIin S3 = 0 S4 = 0
Forward Regenerative Braking	Accel – Decel < 0 & w > Regen Threshold	PIout = Accel – Decel – Iarm BRK = | Accel – Decel – Iarm | * kφ S1 = 0 S2 = 0 S3 = 0 S4 = – PIin
Threshold Reverse Braking	Accel – Decel < 0 & w < 0 & None of the above	PIout = 0 BRK = – | Accel – Decel – Iarm | * kφ S1 = 0 S2 = 0 S3 = 0 S4 = 0
Threshold Forward Braking	Accel – Decel < 0 & w > 0 & None of the above	PIout = 0 BRK = | Accel – Decel – Iarm | * kφ S1 = 0 S2 = 0 S3 = 0 S4 = 0
Freewheeling	None of the above	PIout = 0 BRK = 0 S1 = 0 S2 = 0 S3 = 0 S4 = 0

4.2.3 Mechanical Vehicle Simulation Model

In order for the simulation model to be a useful predictor of the performance of the vehicle, it is necessary to model the mechanics of the vehicle. This model will accept the torque supplied by the motor models of section 4.2.1, apply the road loading associated with the aerodynamic drag and rolling resistance, and calculate the vehicle speed. The basis for this model starts with the well known differential equation for the motion of an object in free space.

$$F_{drive} = ma = m\frac{dv}{dt} \tag{4.9}$$

Where m is the mass of the vehicle (in kg), v is the velocity of the vehicle (in m/s), and F_{drive} is the net force applied at the wheels (in Nm). In addition to this free-body force, there are also the forces of aerodynamic drag (F_{aero}), rolling resistance (F_{roll}), and forces related to the inclination of the terrain ($F_{incline}$) which will affect the vehicle. These forces are collectively called the road load force F_L.

$$F_{aero} = \frac{1}{2}\rho C_d A(v + v_w)^2 \tag{4.10}$$

$$F_{roll} = \mu m g \cos(\alpha) \tag{4.11}$$

$$F_{incline} = m g \sin(\alpha) \tag{4.12}$$

$$F_L = F_{aero} + F_{roll} + F_{incline} \tag{4.13}$$

Where ρ is the density of air (kg/m^3), C_d is the aerodynamic drag constant, A is the cross-sectional frontal area (m^2), μ is the rolling resistance constant, g is the acceleration due to gravity (m/s^2), α is the angle of inclination (rad or deg). In order to make this differential equation easy to apply to the torque Te and angular velocity ω

interface of the PMDC machine models, it will be translated partially into the rotational frame. Equations 4.14 and 4.15 will be used to change the variables in equation 4.9.

$$F = \frac{T}{r_{eff}} \tag{4.14}$$

$$v = \omega \cdot r_{eff} \tag{4.15}$$

$$r_{eff} = (\text{average radius of wheels}) \times (\text{gear reduction ratio}) \tag{4.16}$$

$$\frac{T_{drive}}{r_{eff}} = m\frac{d(\omega r_{eff})}{dt} + F_L \tag{4.17}$$

$$T_{drive} = m\, r_{eff}^{\,2}\frac{d\omega}{dt} + r_{eff} \cdot F_L \tag{4.18}$$

Where ω is the angular rotational speed of the motors (rad/s), and r_{eff} is the *effective* radius of the wheels (m). Notice how the road load force, and its components (which may depend on velocity v), were not changed during this transformation of variables. This gives an equation where the motor torque and rotational speed are available for the machine model interface, while the road load forces will remain in the vehicle speed domain, which has more meaning in the real world.

In order to develop a simulation model from this equation it is necessary to re-arrange the terms so that it can be solved for ω through integration. The end result is shown in equation 4.19.

$$\omega = \int \frac{T_{drive} - r_{eff} \cdot F_L}{m\, r_{eff}^{\,2}}\, dt \tag{4.19}$$

This vehicle mechanical model is implemented as a PSCAD page module shown in Figure 4.5. The page module, along with the connections to the motor models and drives from the previous sections is shown in Figure 4.6.

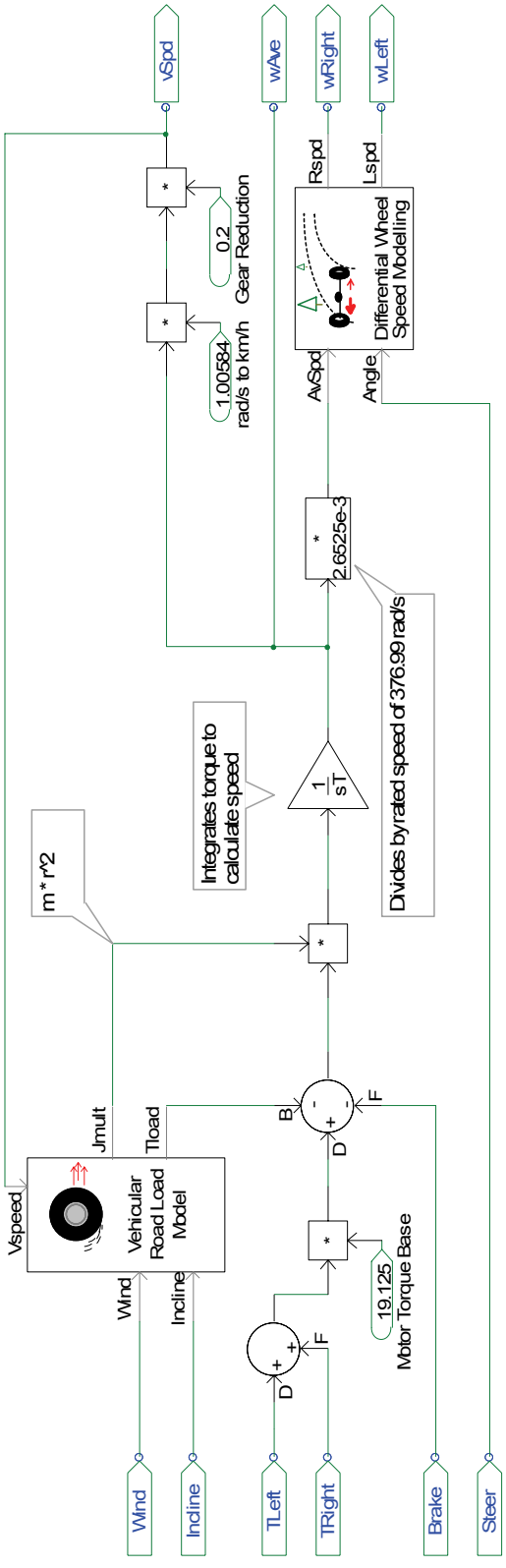

Figure 4.5 - PSCAD mechanical vehicle model page module

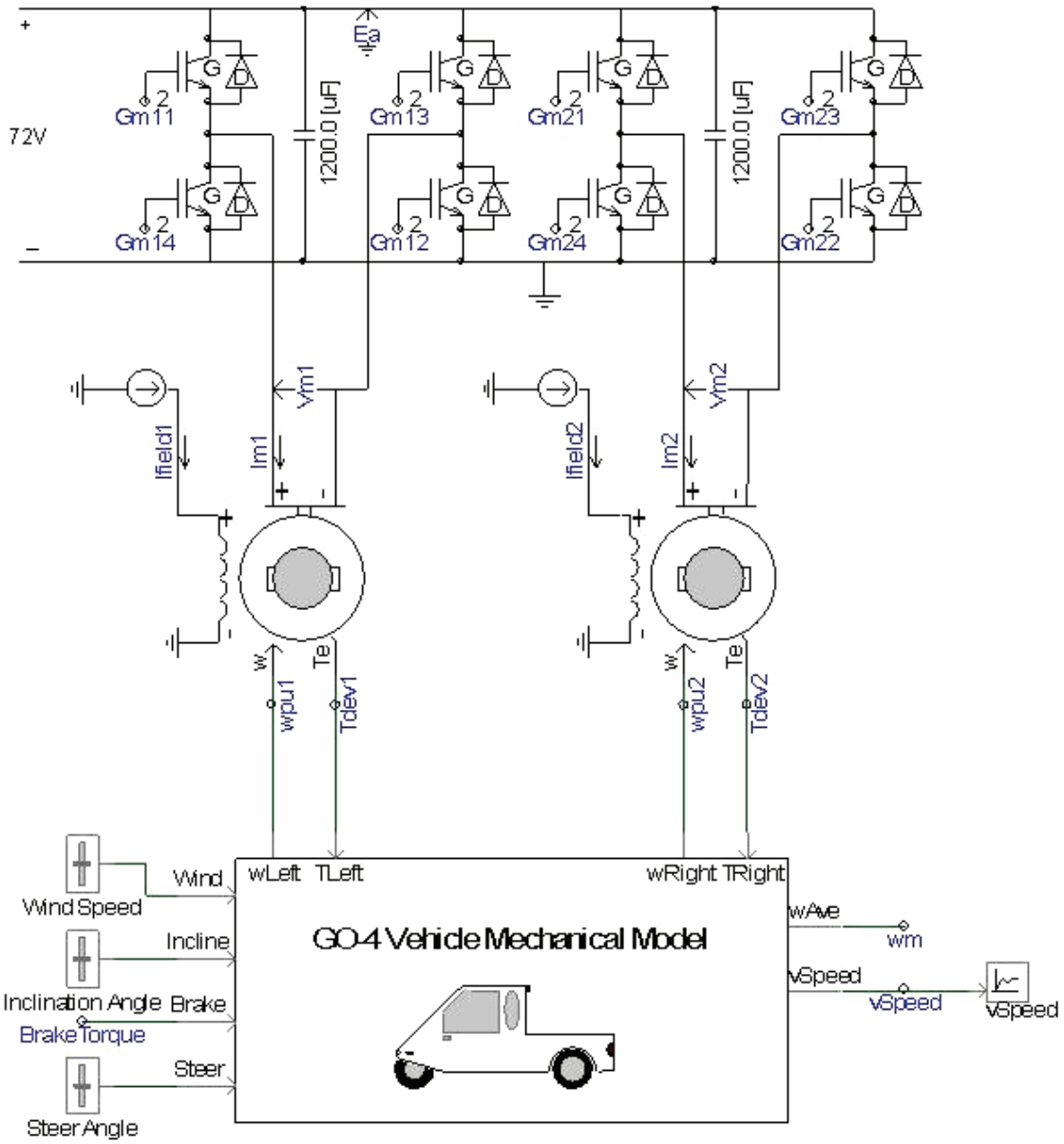

Figure 4.6 - PSCAD model of motors, drives, and vehicular mechanics

As mentioned in section 4.2.2, the motor drive control system calculates the amount of required mechanical braking torque, and applies it to this model directly. The custom block entitled “Vehicular Road Load Model” from Figure 4.5 calculates the load force times the effective radius that is given in equations 4.10 – 4.12, as well as the

quantity (m * r_{eff}^2). The capacitance values of 1200 uF on the DC bus were measured from the terminals of the DMC drive using a multimeter.

Another interesting situation occurs when the vehicle is turning a corner. As the vehicle corners, the outside wheels must travel faster than the inside wheels, since they are tracing out a longer arc on their pass. Since the motors are coupled to each rear wheel independently, a component has been developed to simulate this scenario, which is used in the mechanical model of Figure 4.5. By knowing the angle of the front wheel, it is possible to calculate the relative speeds of the two drive motors by comparing the arc length of the path on which the wheels travel. Figure 4.7 shows the wheel paths as though the vehicle is being driven on a glass platform above the reader.

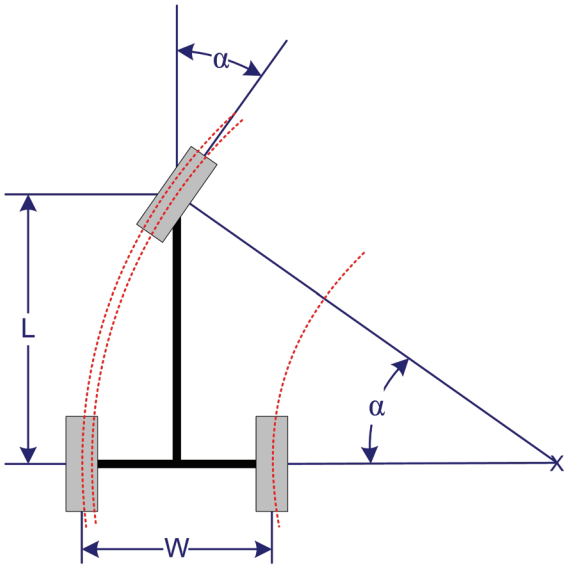

Figure 4.7 - Analysis of wheel speed relationships while cornering

The length *L* (m) is measured from the pivot point at the front axel to the center of the rear axel. The width *W* (m) is taken as the distance from center to center of the rear wheels. The center of the rear axel is taken as the reference point in terms of vehicle speed while cornering. It is then necessary to see how much faster the outside wheel will

travel than this reference point, and how much slower the inside wheel will travel than the reference point. By using Figure 4.7 and some trigonometric relationships, it is straightforward to derive the radii of these trajectories in terms of the physical dimensions defined above and the angle of the front wheel α.

$$r_{reference} = L \cdot \tan(90^o - \alpha) \tag{4.20}$$

$$r_{right} = L \cdot \tan(90^o - \alpha) - \frac{W}{2} \tag{4.21}$$

$$r_{left} = L \cdot \tan(90^o - \alpha) + \frac{W}{2} \tag{4.22}$$

The speeds are proportional to these radii, and since the mechanical model is calculating the speed of the reference point, which is the average speed of the two wheels, the individual wheel speeds are calculated by scaling the respective wheel travel radii against the reference point radii as follows.

$$\omega_{right} = \omega_{vehicle} \frac{L \cdot \tan(90^o - \alpha) - \frac{W}{2}}{L \cdot \tan(90^o - \alpha)} \tag{4.23}$$

$$\omega_{left} = \omega_{vehicle} \frac{L \cdot \tan(90^o - \alpha) + \frac{W}{2}}{L \cdot \tan(90^o - \alpha)} \tag{4.24}$$

Note that these equations have been derived assuming that α is positive when the front wheel is turned in the direction of the right wheel. Note that this assumes perfect tire adhesion to the road, and ignores any over or under steering. Plots of these variations in wheel speed are shown in Figure 4.8.

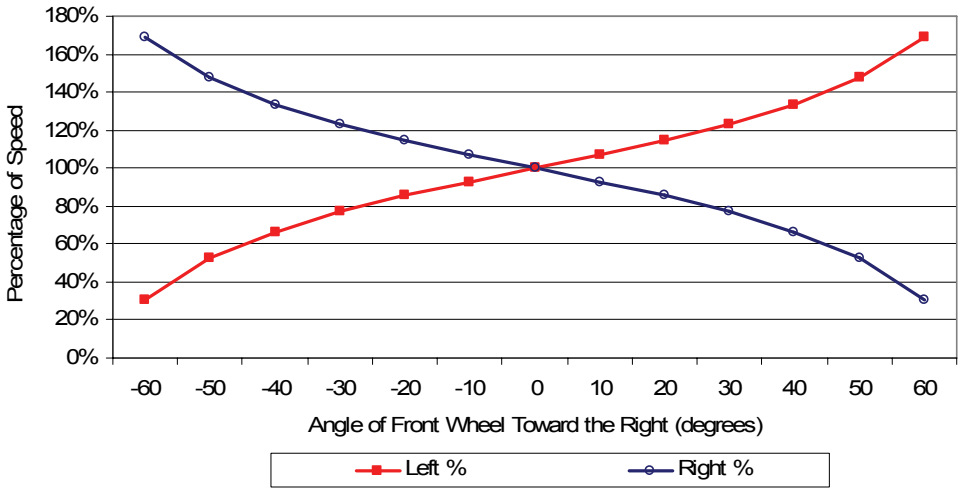

Figure 4.8 - Percentage distribution of wheel speed at various turning angles

4.2.4 Battery Simulation Model

In order to accurately predict the operation of the hybrid vehicle it is necessary to model the terminal voltage variations of the battery bank. There are many different modeling techniques which could be applied to this problem, each with its own advantages and disadvantages, and varying levels of complication. For ease of understanding and simplified application it has been decided to use a simple model which uses an electrical equivalent circuit [16]. This model is shown in Figure 4.9.

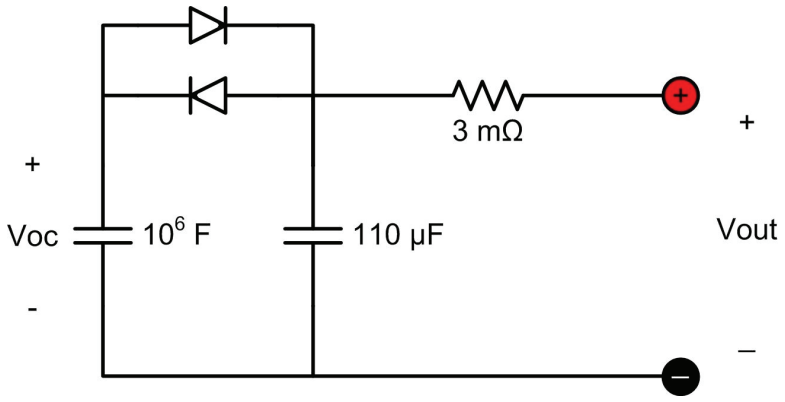

Figure 4.9 - Battery model circuit representation

The circuit shown in Figure 4.9 uses the values given in [16] for a 70 Ah SLI (Starting, Lighting, and Ignition) battery, except for the resistance, which has been taken from the manufacturer specifications in Table 3.3. These battery models are stacked in a series of 6, to model the 6 Optima D35 batteries in the bank. At the beginning of the simulation, the initial open-circuit voltage is applied to the capacitors by briefly switching on ideal voltage sources. Since the diode model in PSCAD assumes a 0.7V forward voltage drop, the 10^6 F capacitor is given 0.7V extra during this process. This circuit is implemented in a PSCAD page module, as shown in Figure 4.10.

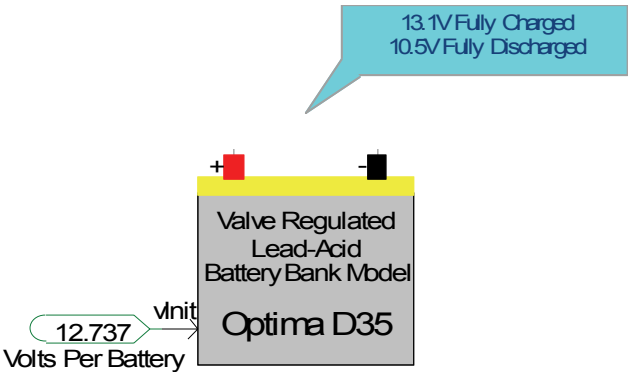

Figure 4.10 - PSCAD page module for battery equivalent circuit

4.2.5 Automatic Drive Cycle Control System

In order to make the simulation model useful for studying vehicle performance in many different situations, it is important that the simulation is able to drive a predetermined course with accuracy and repeatability. Drive cycles have been used for many years as a tool for benchmark testing of such things as fuel efficiency and emissions. Two widely known drive cycles are the EPA's Urban Dynamometer Driving Schedule (UDDS) and the Federal Test Procedure 75 (FTP-75).

The actual end use of the GO-4 vehicle, which is commonly used for parking patrol, does not however resemble these two common tests. Additionally, the top speed of these tests (91 and 90 km/h respectively) makes it impossible to complete for the GO-4, which has a top speed of only 60 km/h. However, there is another common driving cycle with a low average speed and very aggressive stop-and-go style, which is called the New York City Cycle Driving Schedule (NYCCDS). This cycle appears to be a reasonable test for parking patrol, and so it will be used to predict performance in the final application. This test is shown in Figure 4.11.

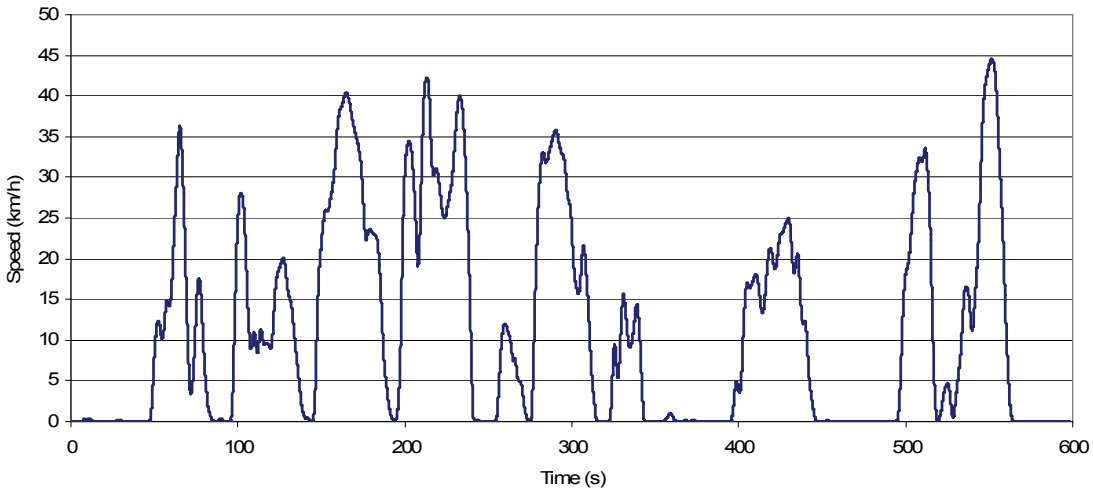

Figure 4.11 - The New York City Cycle Driving Schedule (NYCCDS)

Note that in normal drive cycle testing procedures, ideal road conditions and flat grade are assumed. In order to make the simulated vehicle “drive” this course, it is necessary to allow the computer to control the accelerator and decelerator controls. This will be done using a PI control system, and by reading the reference speed for the NYCCDS from a file. The PSCAD schematic for this control system is shown in Figure 4.12.

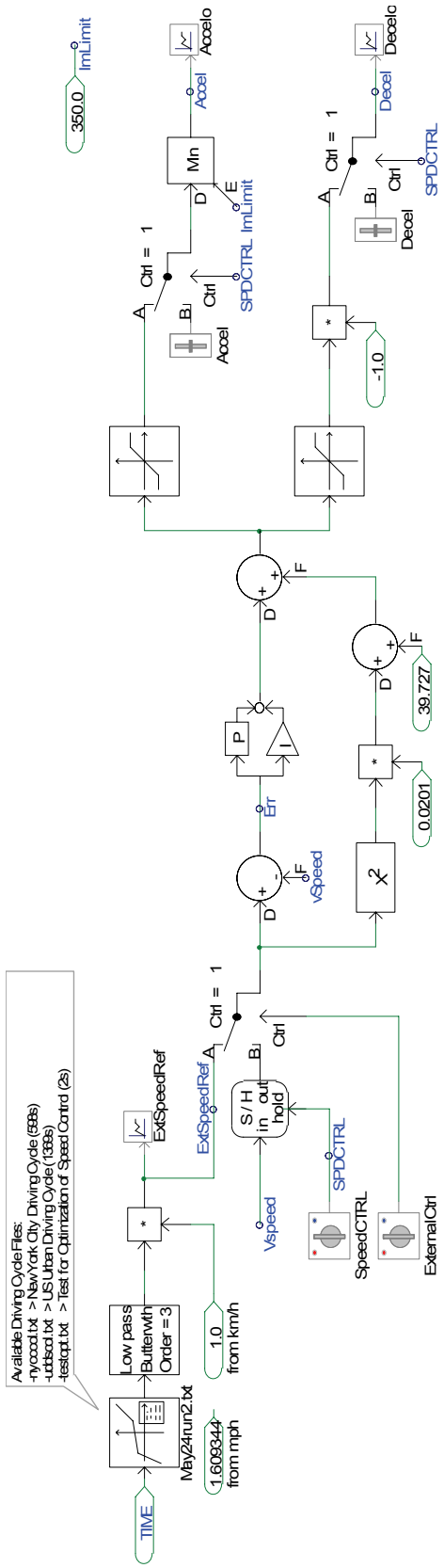

Figure 4.12 - The New York City Cycle Driving Schedule (NYCCDS)

This control system uses a combination of a feedback PI controller and a feedforward calculation. This feedforward calculation was added to increase the stability of the controller while following a drive cycle, and thus reduce the energy consumption calculated by the simulation. The parameters were selected by investigating the amount of armature current required to hold a steady speed with no incline and zero wind speed. This is similar to the calculated static load torque-speed characteristic shown in Figure 3.3. These numbers are a direct result of the vehicular road load model introduced in section 4.2.3, and can also be calculated by using equations 4.10 and 4.11. The PI controller is set up to allow positive and negative output, which allows a smooth transition between accelerating and braking. The positive and negative signals are handled separately as Accel and Decel signals in the drives, and so these are separated by using limiter blocks.

In addition to being able to read an external speed reference from a file, the control system is also able to operate in normal speed control mode, such as the "cruise control" found in many automobiles. Here, a sample-and-hold is actuated when the user selects the SpeedCtrl switch. To select the external reference from a file, the ExternalCtrl switch must also be actuated. Since this simulation has been developed entirely using metric units, a conversion constant is available for use with external files that are in mph. Since drive cycle data is usually available in 1 second time samples, linear interpolation is used for the simulation, and a 3rd order Butterworth filter (0.3 Hz cut-off) is used to smooth the transitions, which will ease the strain on the drive controller. This filter was chosen so that maximum smoothing could be seen, and a minimal change in the envelope of the driving cycle would occur.

4.3 Tuning of the Controllers using Simplex Optimization

There are two systems within this simulation that rely on PI controllers in order to function properly. These are the motor drive control system, developed in section 4.2.2, and the automatic drive control system, which was developed in section 4.2.5. Initially, these PI tuning parameters are selected manually using trial and error until reasonable results were obtained with both systems. Since the automatic drive controller works upstream from the motor drive controllers, the motor drive controllers should be tuned first. Once this has been completed and the system seems to be working as planned, an objective function can be built and optimization can begin. Since the PSCAD simulation is much slower than real time, a short two second drive cycle is designed for use during this optimization. The test drive cycle which has been used for the optimization is shown in Figure 4.13, and the connection of the Simplex optimization block is shown in Figure 4.14.

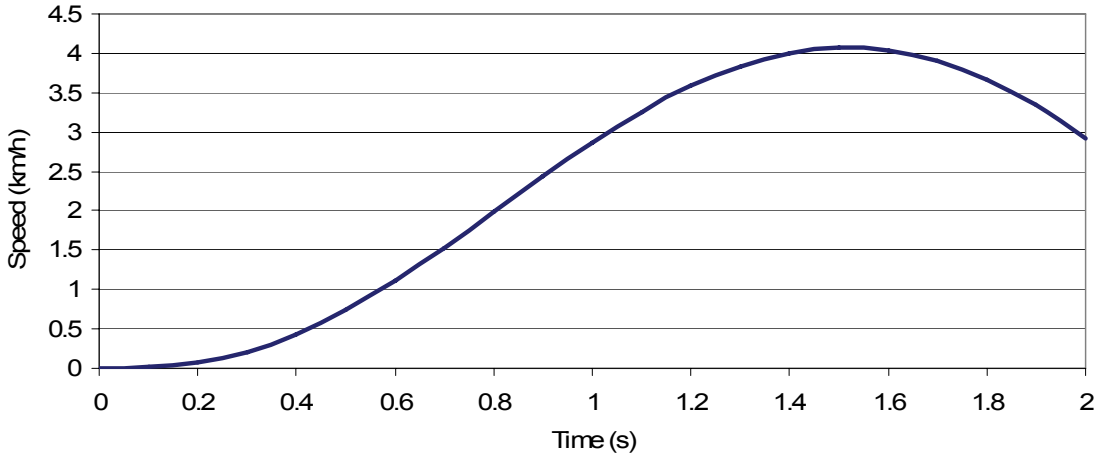

Figure 4.13 - Test drive cycle used for speed and current controller optimization

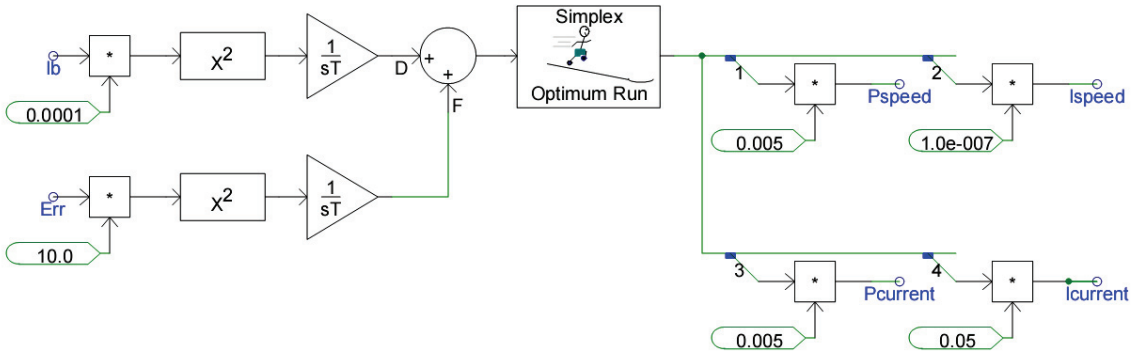

Figure 4.14 - Simplex optimization setup for optimizing speed and current controllers

The test drive cycle requires a hard acceleration at the beginning, and a smooth transition to a medium amount of braking, which is a good test for the speed control system. Obviously any type of drive cycle could be used here, except that simulation time can become too long and potentially provide little benefit. The input scaling and the bounds of the integrators in Figure 4.14 are set to avoid hitting the integrator limits during a run, and also to make the two integrated values arrive at similar values after the initial 2 second test run. The weighting of this input scaling will affect the trade-off in the optimization from the two inputs, which in this case are amp-hours consumed and accumulated speed loop error.

The internal variables for the simplex block will be initialized to 1, and so the initial tuning parameters must be entered by multiplying at the output of the simplex block. This strategy allows each tuning variable to be adjusted in percentage of its initial value, and avoids having the smallest variables being ignored by the algorithm. As an example, the initial value for I_{speed} is 1.0e-007, which is much smaller than P_{speed} (0.005). If the values were not scaled in this way, the I_{speed} could be ignored or adjusted in steps that are too large to see any benefit. The internal settings used within the simplex block

are given in Table 4.3. After 67 runs, the optimization block is able to tune the two controllers to the settings given in Table 4.4.

Table 4.3 - Simplex optimization settings

Setting	Value
Number of real variables to control	4
Maximum number of runs	100
Tolerance	0.001
Initial step size	0.2
All initial conditions set to 1	

Table 4.4 - Results of the simplex optimization

Parameter	Old Value	New Value
P_{speed}	0.005	0.0063
I_{speed}	1.0e-007	2.61e-008
$P_{current}$	0.005	0.00774
$I_{current}$	0.05	0.110
Objective Function	13.456	0.560
Number of Runs	67	

4.4 Evaluation of Simulated Vehicle Performance

As decided in Chapter 3, the top speed of the vehicle is to be 60 km/h. It is important in the marketing of such a vehicle that the performance and capability remain acceptable. The selection of the mechanical gear ratio is important in meeting these specifications, since the top speed is traded off against the acceleration time and hill climbing ability by using this factor, all of which are important performance indices. Therefore an attempt will be made to arrive at the 60 km/h top speed, but not to exceed this. It is also important that this should be possible at battery states of charge that are less than 100%, since generally the vehicle will be slightly discharged.

Determining the top speed of a vehicle with a PMDC drive is not completely straightforward. It is tempting to believe initially that the vehicle speed corresponding to 3600 rpm will yield the top speed. However it is not always possible to match the rolling

resistance, aerodynamic drag, and the frictional forces inherent in the motor and gearbox at this speed. This is because forces such as these quickly increase in a non-linear fashion as vehicle speed increases. These are only the first order effects that will come into play. We will see from the simulation that the battery voltage will dip considerably, both transiently and in the steady state, during an attempt to reach maximum speed. The battery state of charge, or open circuit voltage, is also important. The armature resistance and the wiring resistance between the batteries and motors will play a small reducing role. Additionally, any duty cycle limits inherent in the design of the floating IGBT gate drives of the H-bridge design will introduce limits as well [23]. There are many potential factors which can play a role in the determination of the top speed of such a vehicle. Now that a detailed simulation model taking account of many of these factors is available, the task becomes remarkably simplified.

For this test, multiple gear ratios will be evaluated, and the maximum speed which is arrived at after a reasonable time of 20s will be compared. The initial battery open circuit voltage will be initialized to 12.75V, which corresponds to about 87% state of charge. The motor armature current reference is set manually to 350A, the maximum rating of the drives, and held for the duration of the test. The results for 4:1, 5:1, and 6:1 ratios are shown in Figure 4.15, Figure 4.16, and Figure 4.17, respectively. Notice that it is not possible to hold this setting for very long, as the combination of the rising back-emf in the machines and the dropping battery voltage create a situation where PWM is not able to maintain 350A, and a natural declining armature current is the result.

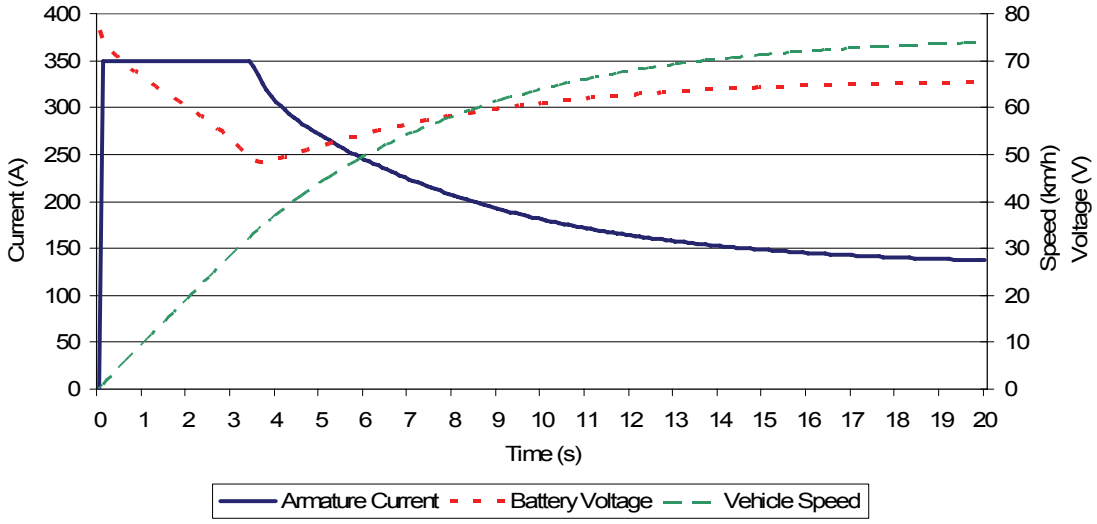

Figure 4.15 - Full acceleration test with a 4:1 reduction gearbox

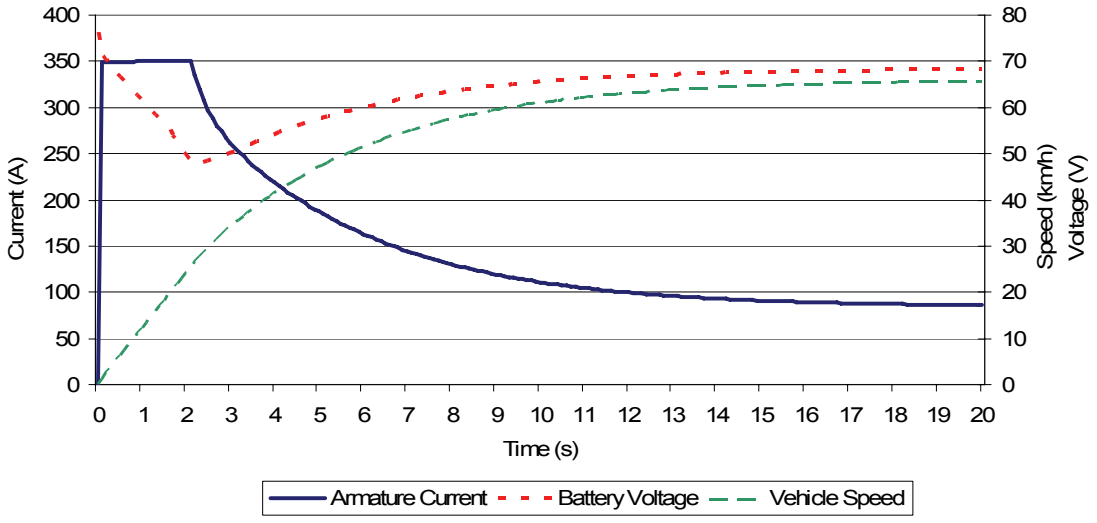

Figure 4.16 - Full acceleration test with a 5:1 reduction gearbox

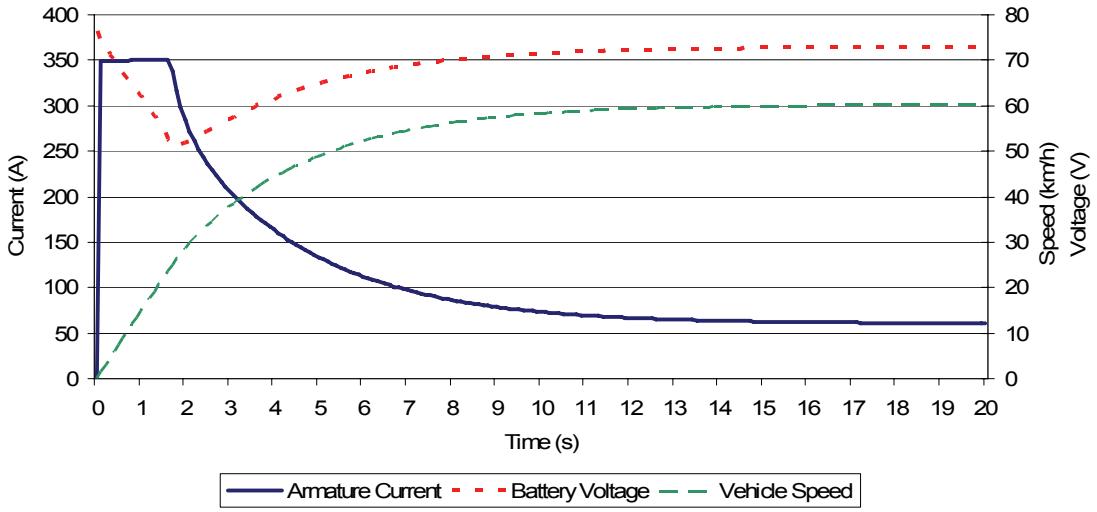

Figure 4.17 - Full acceleration test with a 6:1 reduction gearbox

From the above tests, it is obvious that 6:1 is not a wise choice since it can just barely reach 60 km/h. Notice also that the acceleration for the first two seconds is far greater than required. For a 4:1 gear ratio, the top speed is predicted as 73.8 km/h, which is much too high, while the 5:1 ratio can reach about 65.7 km/h. The ideal ratio then seems to lie between 5:1 and 6:1. However, because it is not easy to obtain such a specific gear reducer without major investment, it is decided to accept the 5:1 ratio. The acceleration test is repeated in Figure 4.18 starting from a full state of charge, 13.1V per battery, and a top speed of 67.3 km/h is predicted. Because it is desired to have some amount of safety margin in meeting this top speed requirement, but also save as much power as possible for hill climbing, the 5:1 gear ratio has been selected.

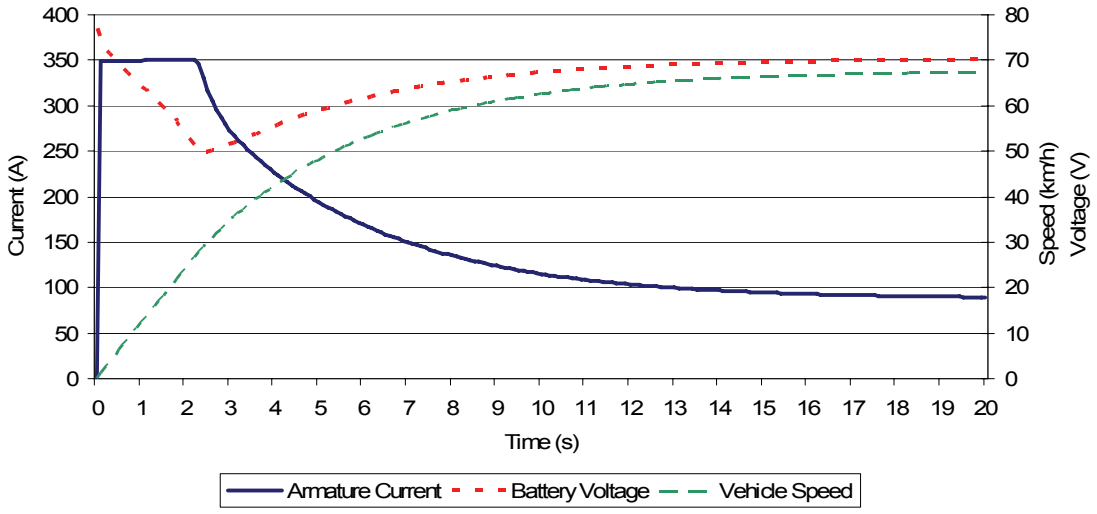

Figure 4.18 - Full Acceleration test with a 5:1 ratio and 100% battery state of charge

In Figure 4.18, it can be seen that the 0-40 km/h acceleration time is 3.7 seconds. This means that we have easily fulfilled the acceleration requirement of 6 seconds. All that remains is to ensure the hill climbing ability will be adequate. Since the mechanical model developed in section 4.2.3 accepts degree angles for the hill steepness, it is necessary to convert the 30% grade specification from Table 3.1, which is common terminology in automotive circles, into an angle in degrees. This can be accomplished by using equation 4.25 [16].

$$\alpha = \tan^{-1}\left(\frac{\%\,grade}{100}\right) = \tan^{-1}\left(\frac{30}{100}\right) = 16.699^{o} \qquad (4.25)$$

This test is done in a similar way, with full armature current reference of 350A, and the incline angle set to 16.699º as calculated above. The results are shown in Figure 4.19.

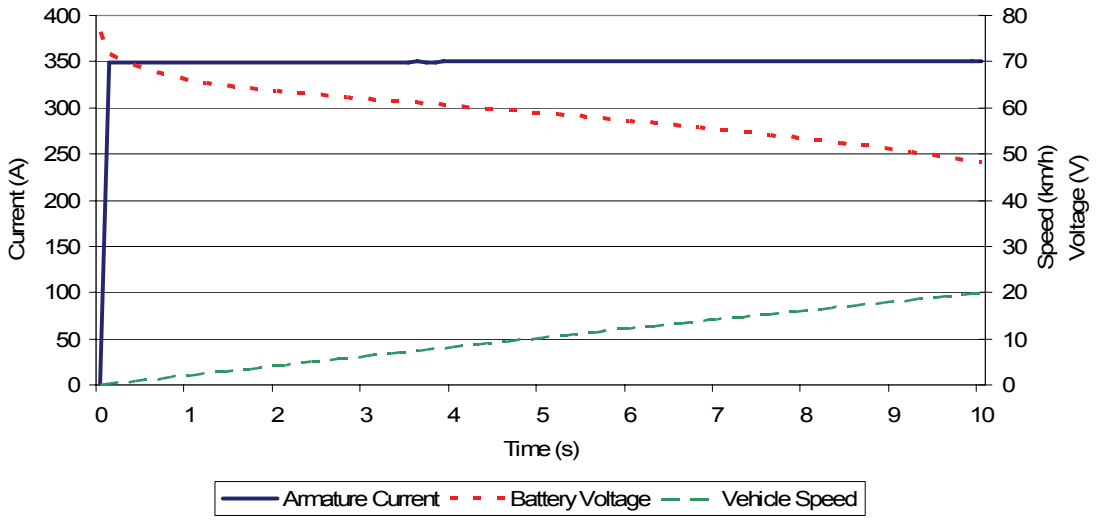

Figure 4.19 - Full throttle acceleration on 30% grade hill climb

As can be seen, the vehicle is able to climb a 30% grade with no major difficulty. However, it is unknown how long this climb with 350A armature current could continue without overheating the motors and the motor drives. Overload protection with a driver warning system should be considered to prevent permanent damage to these expensive components. By using the simulation model, these three tests have predicted the acceptability of the drivetrain design in terms of the performance characteristics from Chapter 3.

4.5 Drive Cycle Testing

The simulation model was tuned in section 4.3 by using Simplex optimization, which resulted in an efficient and responsive armature current controller and a highly efficient and effective drive cycle controller. This system can now be used to drive the vehicle along a speed profile, variable in nature, which is read from an external file. This provides a reliable benchmark test that can be used to evaluate vehicle efficiency, cost of

operation, and potentially the emissions that the engine would produce during a recharge. Essential to this type of evaluation is the idea of drive cycle testing.

A drive cycle could be defined in many possible ways. In general, there are many factors beyond the control of the driver that place constraints on how they will operate the vehicle during a trip, including other vehicles, road conditions, and speed limits. Despite these outside factors, a great deal of liberty still remains for the driver to decide how well the vehicle performs in terms of efficiency. As an example, a person may need to travel along a specified route, shown in Figure 4.20 below. The constraints of this route are listed in Table 4.5.

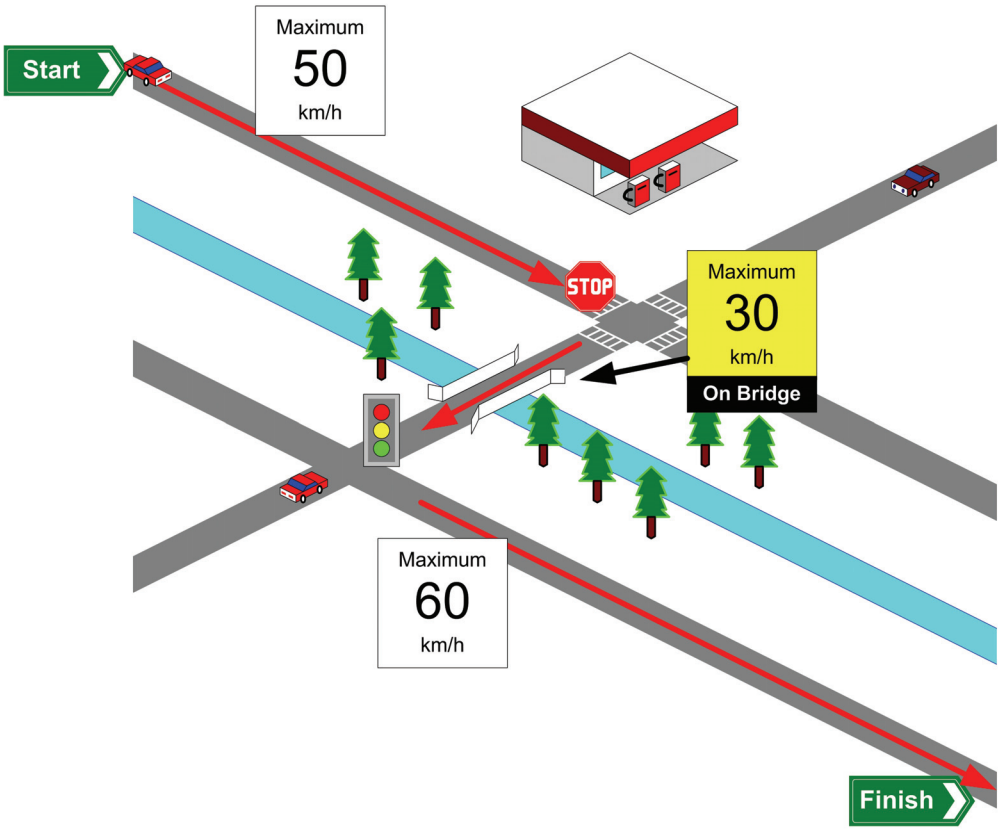

Figure 4.20 - Specified driving route example

Table 4.5 - Specified driving route example constraints

Distance Traveled	Event Info	Next Speed Limit
0 m	Start, wait for 1s	50 km/h
300 m	Stop Sign, wait for 2s, turn right	50 km/h
350 m	Bridge, reduce speed	30 km/h
450 m	Bridge is crossed	50 km/h
500 m	Stop light, wait 5s, turn left	60 km/h
1000 m	Finish, slow to a stop	0 km/h

The above constraints are used with a spreadsheet to generate two example driving cycle profiles. These profiles are given in terms of vehicle speed against time, and follow the constraints listed above. The first example, shown in Figure 4.21 is an aggressive profile. This profile accelerates and brakes quickly, and travels a few km/h above the speed limit while cruising. The second profile, shown in Figure 4.22, is a less aggressive profile which accelerates and decelerates approximately half as hard, and does not exceed the speed limit at any time.

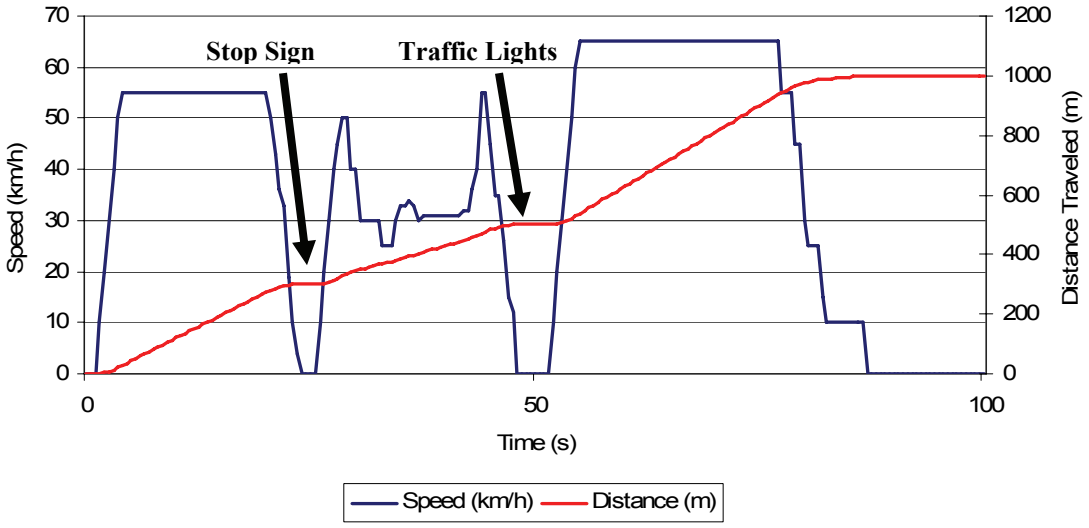

Figure 4.21 - Aggressive driving profile for specified driving route

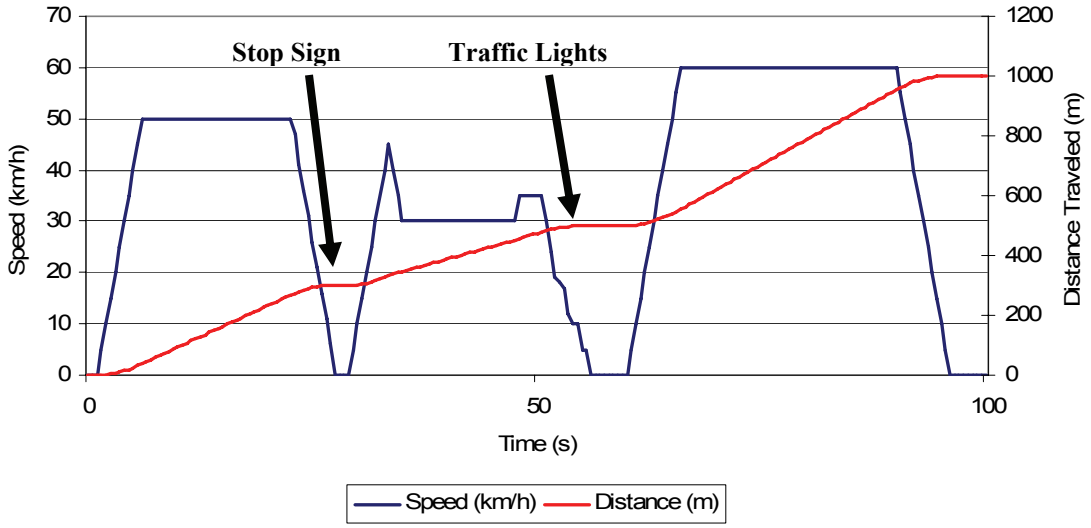

Figure 4.22 - Less aggressive driving profile for specified driving route

As can be seen from comparing the two figures, both profiles travel the same course in similar lengths of time, with the more aggressive driver arriving about 9 seconds sooner, and likely expending much more energy to do so. Note that this test assumes there is no significant wind or incline/decline of the road for this route. This comparison shows that both the distance traveled and the manner in which it is traveled are captured by recording the vehicle speed over time for a given trip. By using this type of data as an input to the simulation model, a specific driving course driven in a specific way is being used, and the aggressiveness of the driver is fully captured.

In order to predict the amount of energy required to travel a given distance, a driving cycle based on speed over time is used. The particular cycle of interest for these tests is the New York City Cycle Driving Schedule (NYCCDS). This cycle is commonly used to test city buses and garbage trucks, which see a great deal of stop-and-go operation just like a parking patrol vehicle. The NYCCDS driving cycle is available on the internet from the EPA website [24]. This test will be done with and without regenerative braking

enabled, in order to predict energy consumption and to evaluate the significance of recapturing this energy. The simulation results are shown in the following figures.

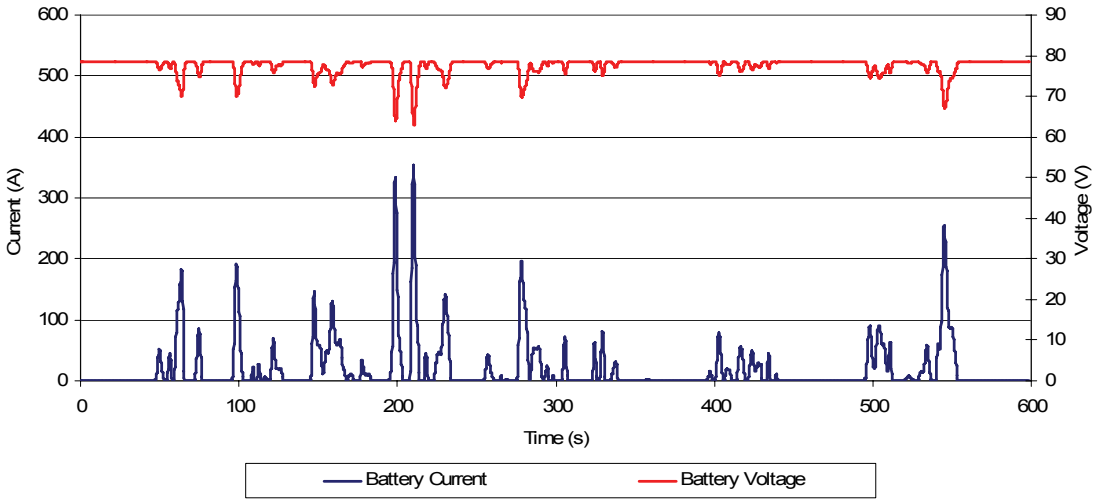

Figure 4.23 - NYCCDS battery current and voltage without regenerative braking

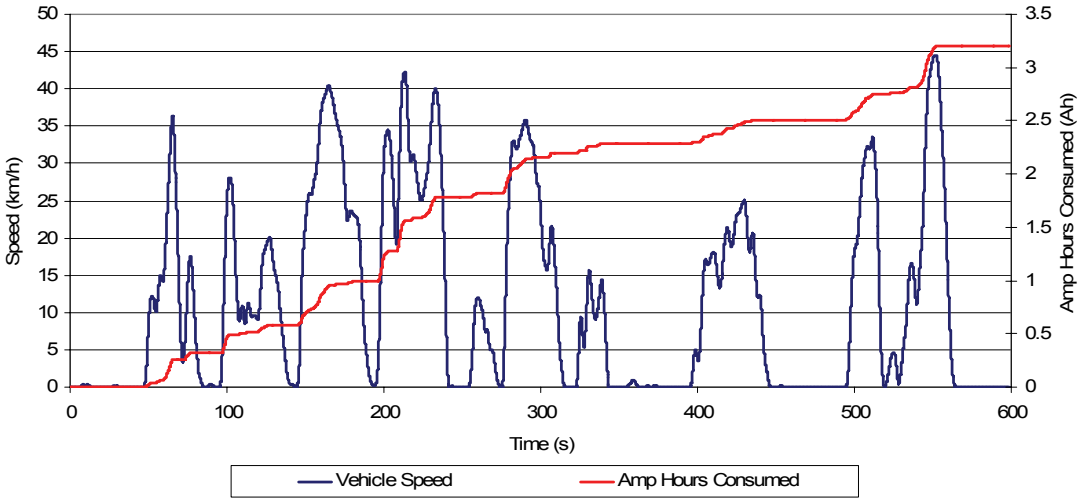

Figure 4.24 - NYCCDS vehicle speed and amp-hours without regenerative braking

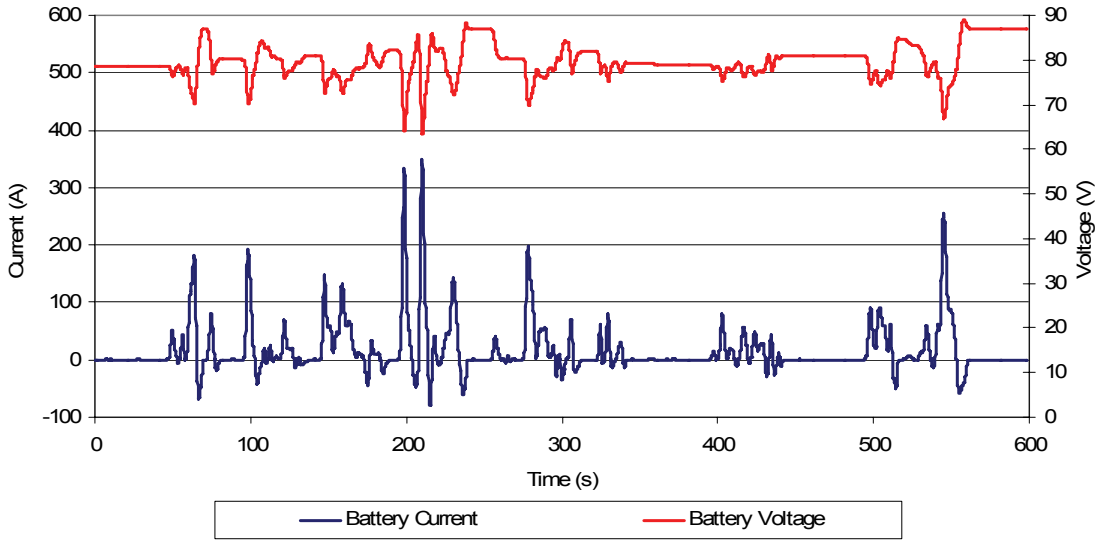

Figure 4.25 - NYCCDS battery current and voltage with regenerative braking

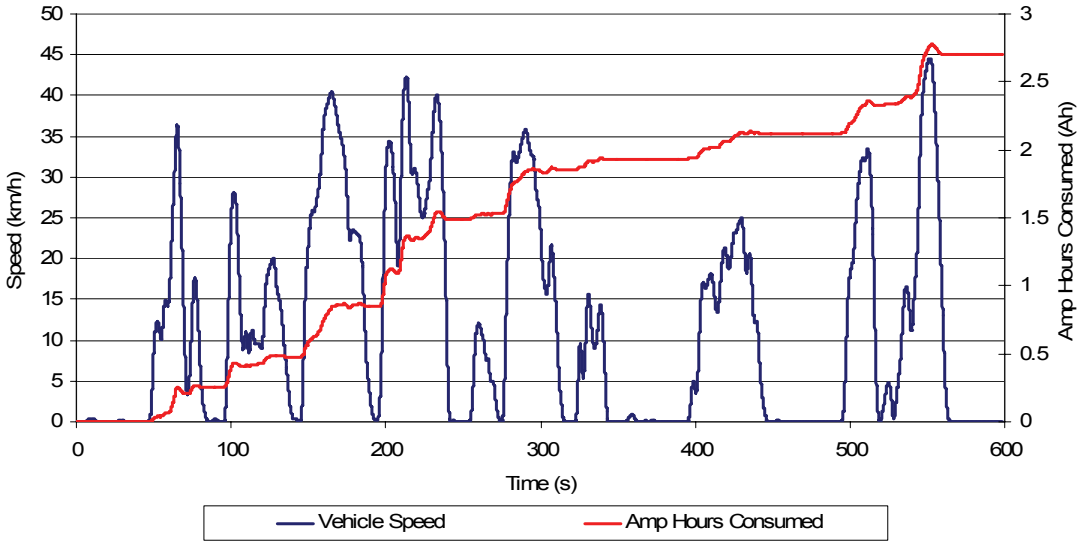

Figure 4.26 - NYCCDS vehicle speed and amp-hours with regenerative braking

As can be seen from the above graphs, the NYCCDS test provides an interesting combination of accelerations and decelerations at different rates, and a great deal of variation of vehicle speed. This means that the drivetrain (and drive cycle controller) is

exercised well during the test. In the case where regenerative braking is enabled, power is continuously flowing into and out of the batteries, and the voltage fluctuates significantly as the battery transitions back and fourth between charging and discharging states.

After performing these simulations, it is possible to see how much efficiency can be gained through the use of regenerative braking, if it were implemented with priority over the mechanical brakes as simulated. More importantly, it is possible to gain an idea about how energy efficient this hybrid drivetrain is expected to be. Some important values gained from this simulation are given in Table 4.6.

Table 4.6 - Summary of NYCCDS tests, with and without regenerative braking

Parameter	No Regenerative Braking	Regenerative Braking	Percent Improvement
Distance	1.8988 km		
kWh	0.2349	0.1951	20.4%
Ah	3.2064	2.6999	18.8%

It is not easy to quantify the meaning of these numbers in a way that is simple to understand. A general metric that is well understood is the miles per gallon (mpg) rating of the vehicle. Generally, this mpg rating is specified over the Urban Driving Cycle and the Federal Test Procedure – 75, which predicts city and highway economy for passenger vehicles. Since this is a different drive cycle, it is not proper to do a direct comparison between the results of this test and these passenger vehicle tests, but bearing this in mind, this figure is approximated in 4.26.

$$\frac{803\ {}^{g}\!/_{L} \times 2.3521 \frac{mpg}{{}^{km}\!/_{L}} \times 0.9 \times 0.9}{\frac{0.1951\ kWh}{1.8988\ km} \times 300\ {}^{g}\!/_{kWh}} = 49.6\ mpg \tag{4.26}$$

Where 803 g/L is the density of gasoline, 2.3521 is the conversion between km/L to mpg, 0.9 is assumed as the efficiency of both the generator electric system and battery

charging, and 300 g/kWh is assumed for brake specific fuel consumption of the engine. Note that this mpg figure is measured in US gallons, which is less an imperial gallon. The imperial measurement corresponding to this is about 59.6 mpg, but since the vehicle will be sold in the US only, the US figure will be used for all further discussion. This calculation ignores the energy consumed by any auxiliary electrical loads in the vehicle, such as the headlamps, brake lights, stereo, fan, or air conditioning. Another inaccuracy is the fact that coastdown parameters were taken from the gasoline drivetrain, which may be different for the hybrid drivetrain.

This leads us to expect that the hybrid drivetrain will be much more efficient than its gasoline predecessor for parking patrol. However, there are many things which are not accounted for in this analysis, and verification of this simulation model against a prototype vehicle would give much more weight to these results.

5 CONSTRUCTION OF A PROTOTYPE VEHICLE

5.1 Summary

With the insight gained from the simulation model developed in Chapter 4, it can be said that an electric-only GO-4 built with the components specified in Chapter 3 should meet or exceed all the performance requirements for parking patrol, except possibly the desired range. With the series hybrid design, it is possible to add an engine and a generator to the electric drivetrain to extend the driving range, and thus guarantee this requirement will be met as well. This chapter will detail the construction of a prototype very similar to the simulation model, which will also be electric-only. Chapter 6 will then analyze the differences between the simulation and prototype, and will reconcile and give explanations for them.

5.2 Interfacing the PMDC Motor Drives

According to the US Federal Motor Vehicle Safety Standards (FMVSS), which the GO-4 is obligated to meet, the design choices made so far dictate that the vehicle battery system must be electrically isolated from the frame [15]. This poses some challenges from a control point of view, which will have to be overcome by design. Utilizing an isolated dc/dc converter for the 12V supply system allows the normal automotive devices to be powered from the main 72V battery, and meet this requirement without a problem. However, where control signals must pass from such a device to the electric drive system, special consideration is required. This important rule must be kept

in mind while designing all portions of the control system that will interface with the drive system.

Another challenge is to interface the two motor drives so that they will properly distribute torque to each rear wheel. In a normal automobile, this task is handled by the use of a differential. The differential, under normal operation, distributes equal torque to each wheel, regardless of the individual wheel speeds [19]. This excludes cases where the friction coefficient (μ) significantly varies between the drive wheels, and/or when the vehicle is in a skid. With this strategy, more power is directed to the outside wheel during cornering, and less to the inside wheel. Equal torque distribution is easy to apply using dc electric motors, since the torque is proportional to the armature current, and is simple to control. To accomplish this, the motor drives will be set to operate in current control mode [22].

The torque control input of the motor drive is designed to accept a 0-5 kΩ potentiometer. Because of the potential problems associated with wiring these inputs in parallel, and because a fine level of control is desired, it is decided to use other means to accomplish this task. Two digital potentiometers, each controlled separately by an onboard microcontroller, will perform this balancing task. The microcontroller will be responsible for reading the accelerator pedal position, along with other inputs from the vehicle, and to provide the correct signal via the digital potentiometers. For example, provisions have been made for reading the angle of the front wheel, so that in the future a more active torque balance control system could be attempted. This accelerator pedal potentiometer circuit is naturally isolated from the frame ground. A schematic of this system is shown in Figure 5.1.

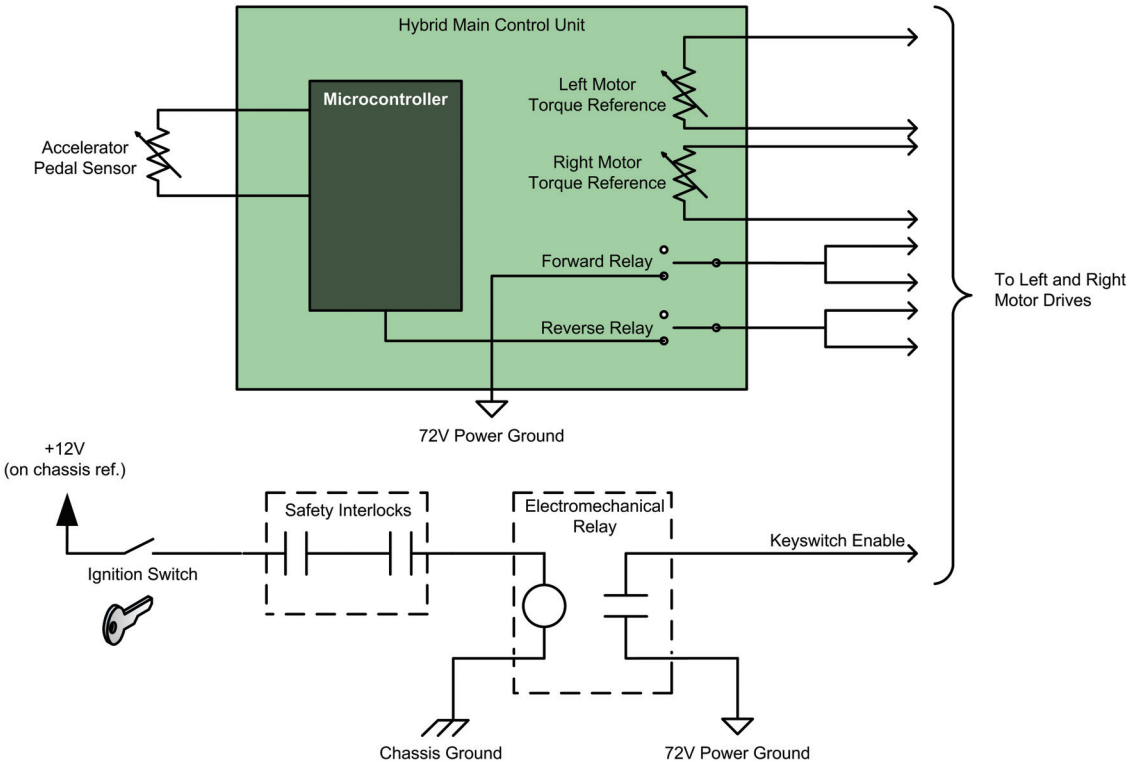

Figure 5.1 - Wiring schematic for interfacing the DMC motor drives

Another input to the motor drives is the selection of forward and reverse. Each of the motor drives provides inputs weakly driven to a high state, which are asserted by externally grounding them to the negative dc bus with a simple mechanical switch. Separate inputs are used for forward and reverse. With this scheme, the drive can identify a wiring problem by checking that only forward or reverse can be selected at one time. Additionally, there is a power-up timer which will trigger a failure state if a selection is made before the drive is powered up. These forward and reverse inputs will be triggered via the onboard microcontroller through two separate electromechanical relays. The two inputs, since they are weakly driven by each drive (through some impedance), can safely be connected in parallel. Electromechanical relays allow appropriate electrical isolation between the drive and the frame or control circuit. The method in which the

microcontroller obtains the driver selection for forward and reverse will be explained in sections 5.4 and 5.5.

It is required to use a similar sinking type input as an enable signal for each drive. This is more commonly called the key-switch. This line must be grounded to the negative dc supply to enable the drive to function. Since this project will be interfacing the existing automotive systems in the vehicle, such as a standard ignition switch referenced to vehicle ground on a 12V dc system, another electromagnetic relay is used here to change voltage references and maintain the necessary isolation. Any safety interlock contacts, such as the onboard charger or an additional emergency cut-off switch, are added in series with the 12V coil circuit.

5.3 Hybrid Main Control Unit

Since the design of the DMC motor drives and the method by which they are to be used necessitates an onboard microcontroller system, it is worthwhile to combine many other control functions and features into this unit, called the Hybrid Main Control Unit, or simply the main controller. Since this is a prototype vehicle, which will be used to gain knowledge of its operation and to verify this against the performance of the simulation model of Chapter 4, monitoring functions are quite useful. Battery voltage, battery current, user throttle input, and the left and right rear wheel speeds will be measured by the main controller. It will also read the user throttle position, send the left and right torque commands, and select the forward and reverse modes for the two DMC drives.

The battery voltage is measured by using a resistive divider and analog optocoupler circuit as shown in Figure 5.2. The optocoupler is not entirely necessary, except that it provides some safety from any battery circuit transient voltages from

damaging the controller. The battery current is measured using a chassis-mounted hall-effect current sensor. This sensor is linear in the range of -600 to +600 amps dc. Details of this circuit are also shown in Figure 5.2.

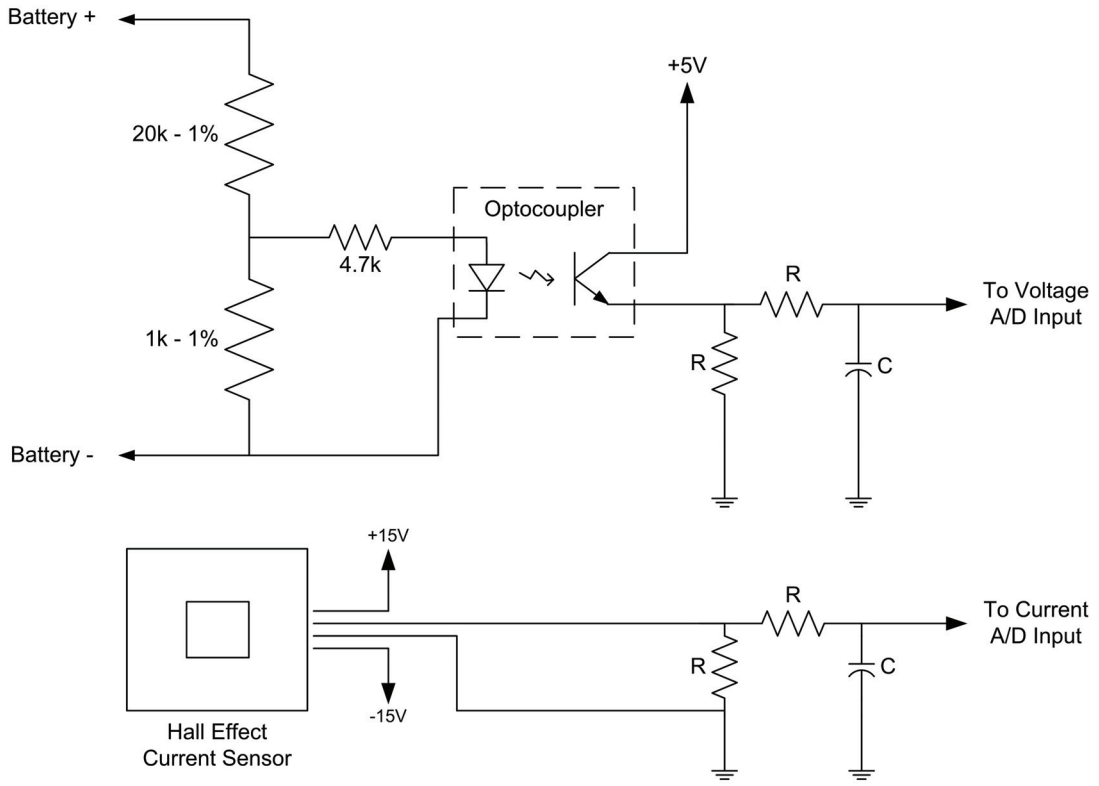

Figure 5.2 - Battery voltage and current measurement circuitry

The left and right wheel speeds are measured by using a hall-effect vane sensor and metal gear-tooth mounted on the driveshaft. There is a simple RC filter on the input to prevent high frequency noise from affecting the pulse count. This pulse count is fed directly into two onboard 16-bit microcontroller timers, which are operated as counters with an external clock. By checking the number of pulses at repeatable increments, a number proportional to the rotational speed of each wheel is obtained.

It is not strictly a simple matter to control an electromechanical relay from a CMOS microcontroller digital output. The amount of current required to do this will put stresses on the controller, and can cause large fluctuations in the power to the controller, possibly causing nuisance reset problems. Therefore, a BJT is used to drive the coils of the relays directly from the power supply rail. An RC filter at the base of the transistor is used to slow the speed of operation of the relays, to keep transient effects on the power supply rail to a minimum. A schematic of this circuit is shown in Figure 5.3.

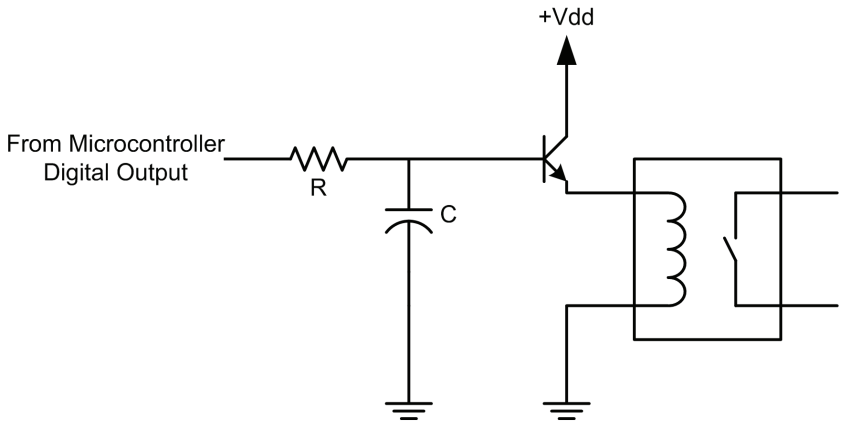

Figure 5.3 - Schematic of relay drive circuit

5.4 Shifter Input Hardware

As mentioned earlier, it is necessary to devise a method for collecting the user input for forward, reverse, and neutral states of operation. After considering many other options, it was decided to use a standard automatic transmission gear shifter for this functionality. This would help make it more familiar to the end users, who may be worried about the prevalence of electronics in the drive system.

To accomplish this, a special microcontroller based sensor input board was designed. This board uses magnetic hall sensors to sense the position of the shifter at each of its set positions. A south pole magnet is mounted to a moving portion of the shifter handle, to actuate these sensors. The position information is then sent through a serial CAN link to the main controller, where the appropriate action is taken. The CAN communication link is discussed further in section 5.5.

A standardized CAN message, which is dependant on the position of the shifter, is sent every 0.25s or sooner if this position is changed. The actions to be taken are the responsibility of the main controller. For the prototype, Park, Neutral, Reverse, Drive, 2, and L (low gear) work similar to a normal automatic transmission, with Drive, 2, and L corresponding to forward motion without any change in speed. With the future addition of the engine to the system, these positions can also be used to enforce all-electric operation, force the engine to remain running, or to allow mixed-mode on and off operation of the engine. Because this is easily adjustable in software, special customer requirements could also be met by changing the function of these shifter positions. Pictures of the prototyped shifter are shown in the following figures.

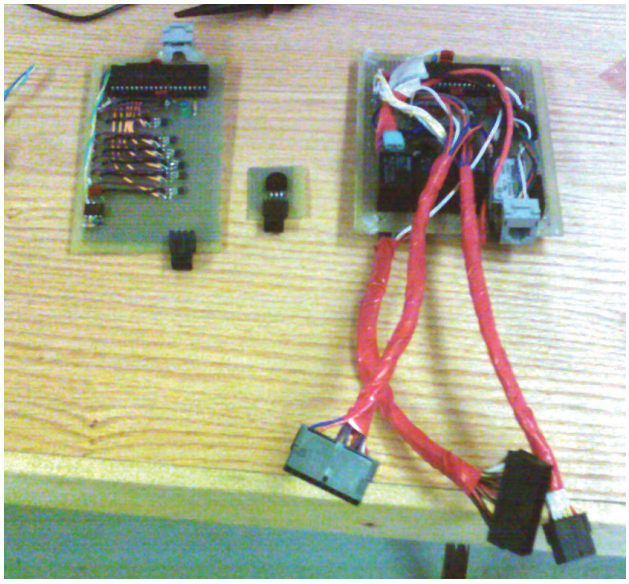

Figure 5.4 - Shifter circuit board (left) and main controller (right) prototypes

Figure 5.5 - Shifter circuit board installed within the shifter unit

5.5 CAN Bus Communication

As mentioned in earlier sections, a serial communications protocol called Controller Area Network (CAN) has been implemented in the vehicle for communication between controllers and for data logging or diagnostic purposes. CAN is most often implemented in conventional automobiles under the auspices of a higher level protocol known as SAE J1939 or OBD2. This implementation uses a proprietary but simple higher level protocol where controllers simply broadcast information on periodic intervals, and any other interested hardware on that bus will receive and react to this information. The speed of communication is 250 kbps, and the extended (29 bit ID) is used exclusively. The two important data transmissions which are made on the bus are summarized in Table 5.1.

Table 5.1 - CAN bus data transmissions

CAN ID	Sender	Frequency	Data Bytes	Data Bytes
12.90.128.129	Main	0.1s	8	Throttle Pos., Battery Volts, Battery Amps, Steer Angle, Brake Pos., Left Speed, Right Speed, Not Used
12.90.129.128	Shifter	0.25s	1	Shifter Position

The shifter position transmission is the most important piece of information being transmitted on the bus. If a sufficiently long period of time passes without receiving a shifter position update, the main controller must take appropriate action for the safety of the driver, which means placing the drives in neutral. The main controller transmission is for diagnostic and data logging purposes only. In the future, it is planned to develop a CAN-enabled dashboard display unit for the cluster of the vehicle, which would use both these data streams to display relevant information to the driver. The possibility to have multiple users of the same broadcasted information is an important strength of CAN in

this type of application, as it reduces the cost and complexity of wiring considerably. CAN, which was originally developed for use in motor vehicles, is a fault tolerant and reliable form of serial communication.

5.6 CAN Data Logging Software

An important use of the CAN bus during development is for data logging. In order to effectively compare the prototype vehicle's operation against the simulation model, a simple form of data acquisition and logging is required. Since the main controller is broadcasting most of the relevant information over CAN, it makes sense to simply record this data with a laptop computer. Custom developed PC software was developed using Microsoft Visual Basic .NET 2005. The laptop is connected to the vehicle CAN bus through a CAN to USB adaptor dongle.

The program simply waits for the occurrence of CAN messages on the bus and plots the values to a graph on the screen. The graph is composed of 8 different plot channels, each of which is configurable to be linked to a different CAN ID and data byte. The individual CAN bytes are 8-bit values, and these data bytes are interpreted as a double value from 0-255. A facility is also provided to apply a gain and offset adjustment in order to calibrate this value into the proper units for display. Finally, once the data acquisition is stopped, a facility exists to write the data to a Comma Separated Value (CSV) file, which can be opened and processed in a spreadsheet or other data analysis program.

The shifter position and vehicle speed are shown along with the dynamic graph. The displayed vehicle speed is calculated by the program as the average of the two measured wheel speeds. Although the graph portion is fully configurable by adjusting the

gain, offset, and CAN ID for the message to be captured, these two additional pieces of information are hard-coded into the program for simplicity. A screenshot of the developed software is shown in Figure 5.6. The "Calibrate Input Channels" button brings up a dialog window with the calibration parameters, which are saved and persisted. This window is shown in Figure 5.7.

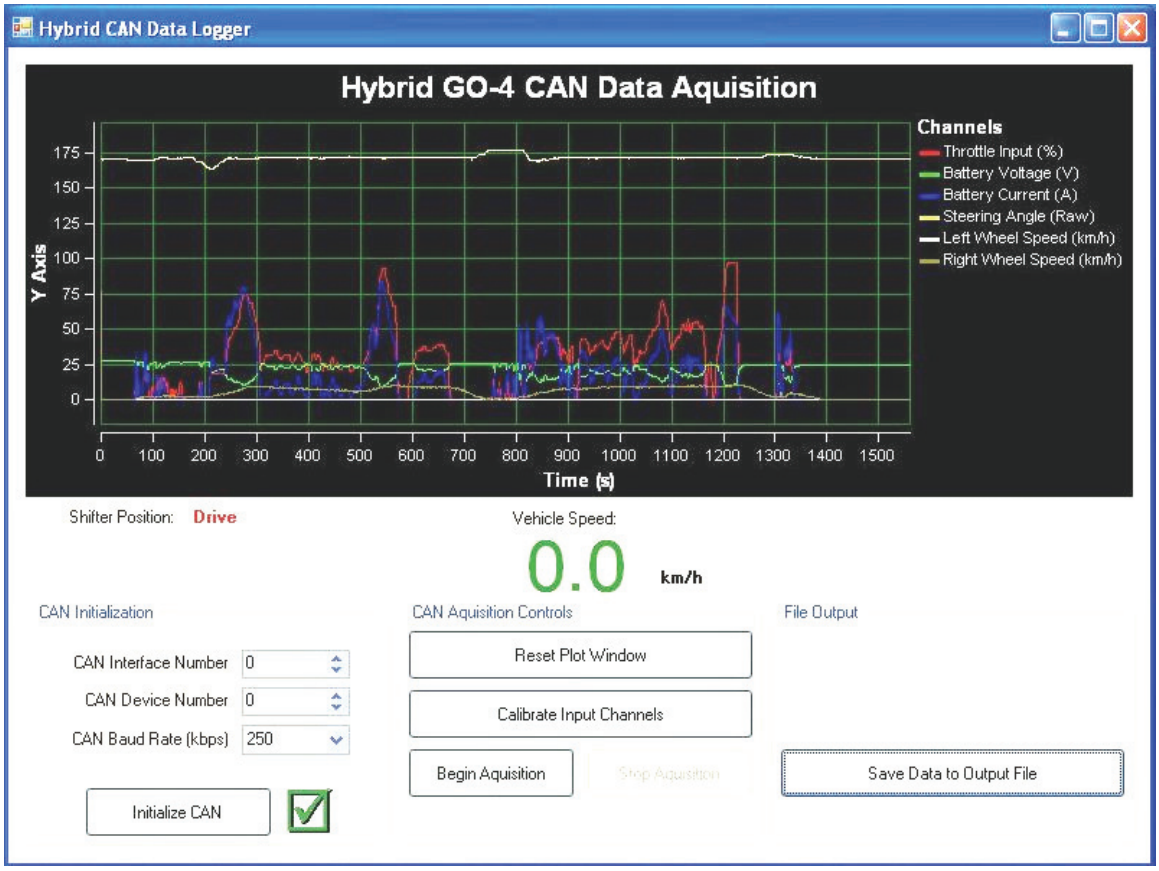

Figure 5.6 - Screenshot of the CAN data acquisition PC software

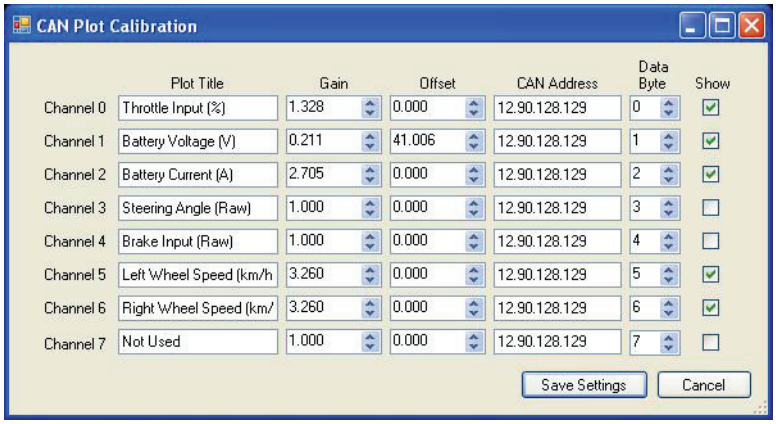

Figure 5.7 - Adjustment window for the calibration parameters

5.7 Implementation

The control circuits and components are installed into a standard chassis for a current model GO-4. The batteries are located below the seat in a central, low location to give the vehicle a low center of gravity. The motors are assembled into a package with the 5:1 ratio planetary gear heads as shown in Figure 5.8. This package is mounted on an angle of 20 degrees to allow the CV (constant velocity) drive shafts to operate within the appropriate bending range throughout the suspension travel. The main controller is installed inside the wiring box of Figure 5.9. All drivetrain connections are made using the terminal blocks to allow easy troubleshooting and modification. Two dc electromagnetic contactors are used by the individual drives for a safety cut-off, and a spare is shown mounted for the future addition of the engine and generator. A 400A semiconductor fuse is installed for safety.

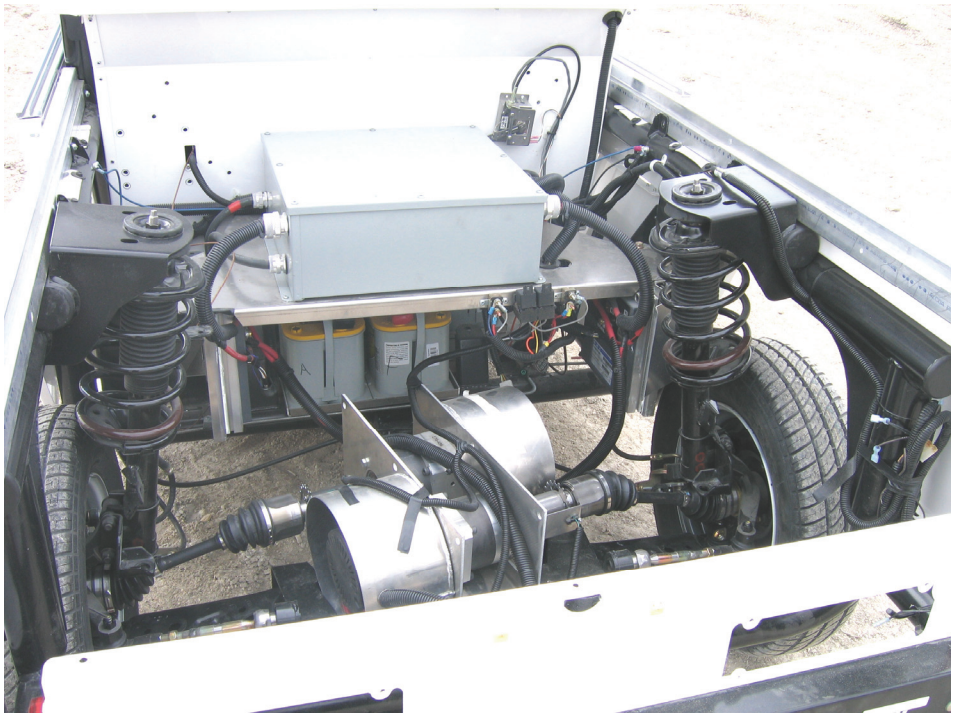

Figure 5.8 - Rear view of prototype vehicle

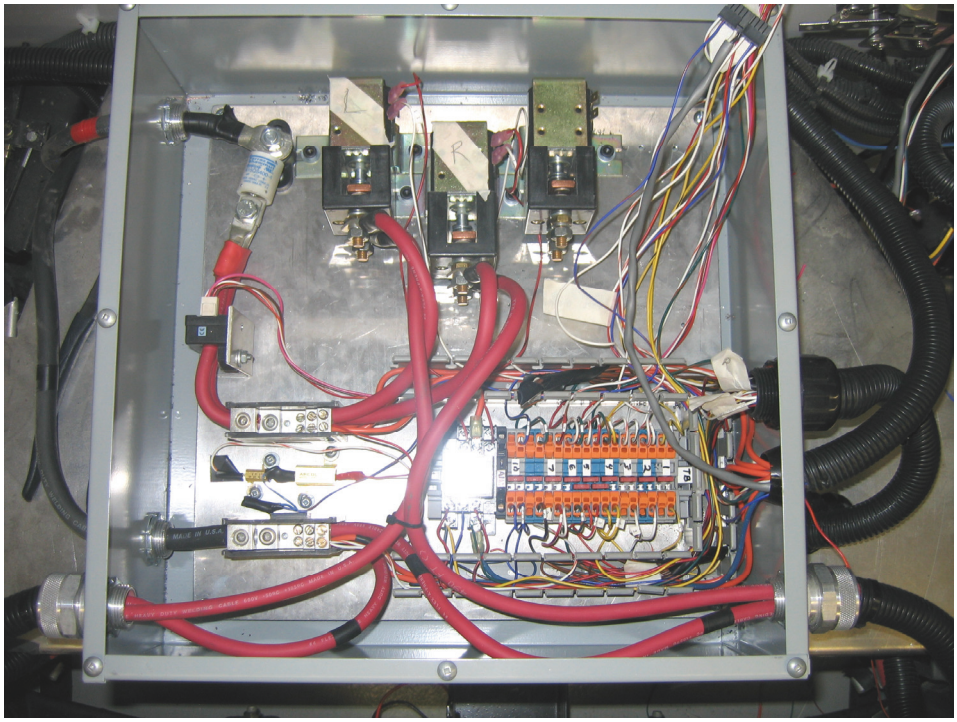

Figure 5.9 - Power and control wiring for prototype vehicle

Figure 5.10 - Side view of prototype vehicle

6 VERIFICATION AND RECONCILIATION

6.1 Introduction

Chapter 4 has presented the development of a highly detailed computer simulation model of the electric drivetrain. Chapter 5 has detailed the design and construction of a prototype vehicle with this drivetrain. In this chapter, efforts will be taken to ensure the parameters of the simulation model are accurately adjusted to match the prototype, and then a comparison of the simulation model and prototype will be made. How well the simulation model can predict the performance of the prototype is important for evaluating its use for future design and refinement needs.

6.2 Calibration of Data Logging Software

As presented in Chapter 5, data logging software running on a laptop computer has been developed in order to capture test drive data and save it for later analysis. However as with most 8-bit microcontroller applications, data is stored in such a way to maximize the efficiency and accuracy within the 8-bits allowable. Therefore the numerical results which are captured from the CAN bus must be scaled and offset by using the appropriate calibration parameters.

The battery voltage and current were calibrated by taking measurements of different values with the use of hand-held meters. Different battery currents were tested by pressing the accelerator pedal different amounts with the emergency brakes engaged. Throttle input was scaled to vary from 0 to 100% when the pedal is pressed and released. Vehicle speed calibration requires an actual test drive to be done, and an alternate method

of measuring and recording speed. For this task, a commercially available onboard GPS logging device was used. By comparing the data from the GPS device and the captured speed trace from the laptop, the appropriate calibration parameters were found. An example showing the fit of the two data sets is shown in Figure 6.1. Notice that the speed recorded from the vehicle will require some filtering before it can be used as an input to the simulation.

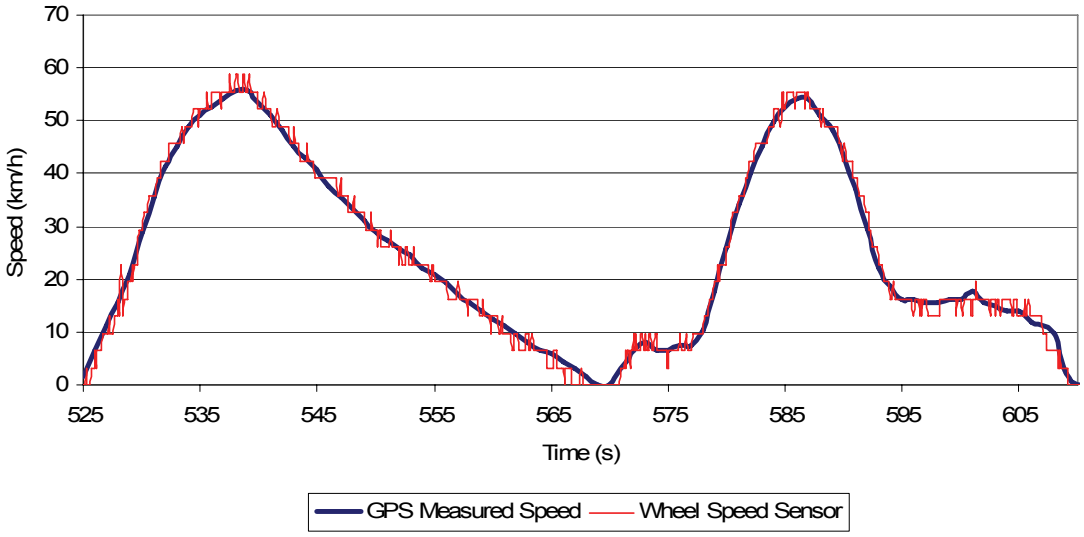

Figure 6.1 - Calibration of the vehicle speed for data logging application

6.3 Coastdown Test

As detailed in Chapter 3, a coastdown test was done on an existing gasoline powered GO-4 vehicle for the purposes of early design calculations. Now that a GO-4 with the electric drivetrain has been constructed, a new coastdown test is done using this prototype. From this coastdown test, the true values for the rolling resistance and aerodynamic drag coefficients can be obtained. The same process is followed as explained in Section 3.2, but this time using the data obtained from the GPS data from Section 6.2. The results of this process are shown in Figure 6.2.

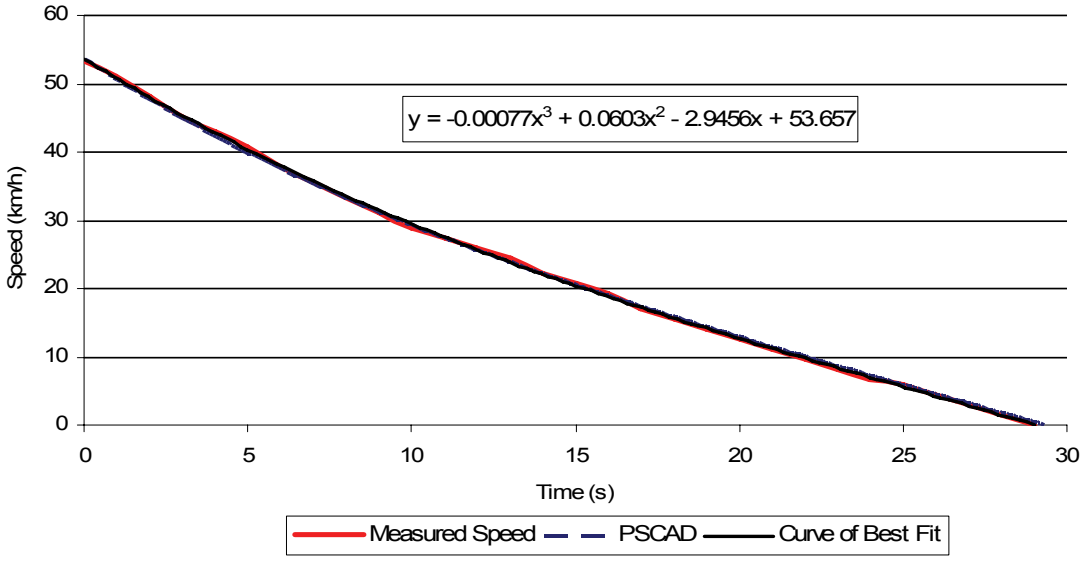

Figure 6.2 – Coastdown speed data for prototype vehicle (CDA = 2.467, μ = 0.0381)

The calculated values for CDA and μ have been tested in the PSCAD simulation by doing a simulated coastdown test, and the results, which are also shown in Figure 6.2, are in good agreement with the line of best fit.

6.4 Test Drive Data

Now that the simulation mechanical model parameters have been experimentally determined, an attempt will be made to judge the accuracy of the simulation model against data measured from the prototype. The method employed will be to drive an arbitrary course using the prototype vehicle, and then feed the captured speed data into the simulation model to generate comparisons for the battery voltage and current consumed. The energy consumed during the trial will be compared as well. The results of this comparison are shown in the following figures.

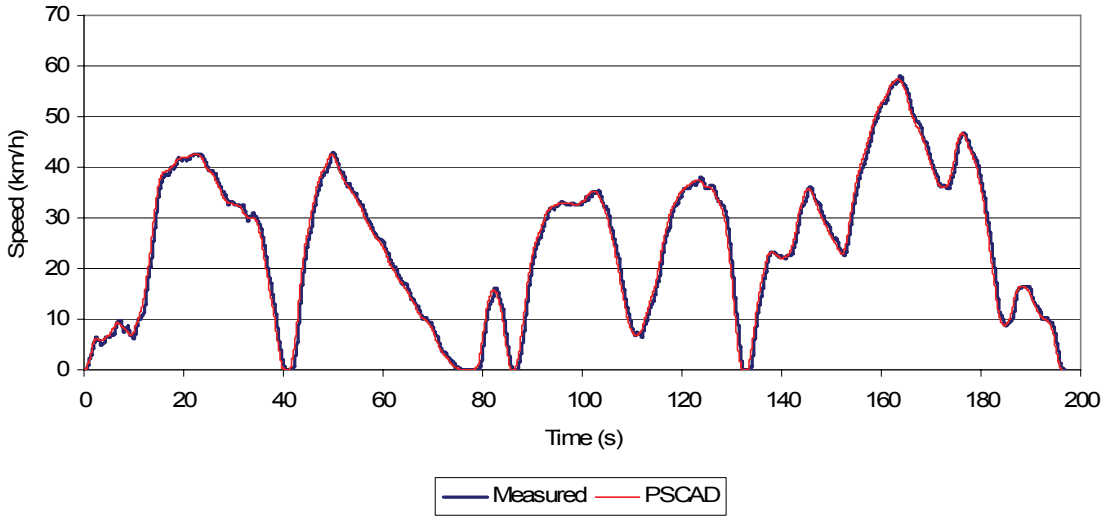

Figure 6.3 - Vehicle speed from prototype and simulation model

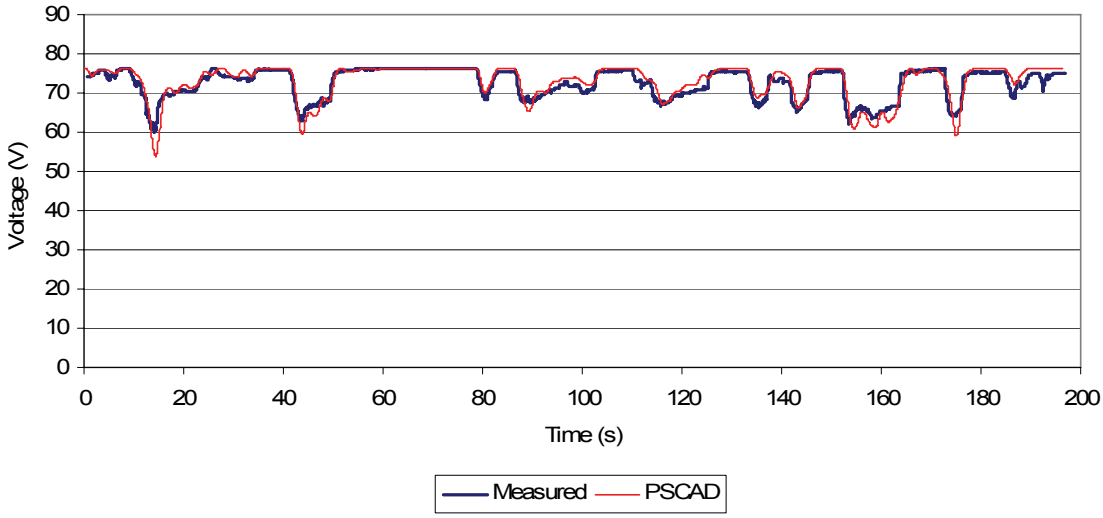

Figure 6.4 - Battery voltage from prototype and simulation model

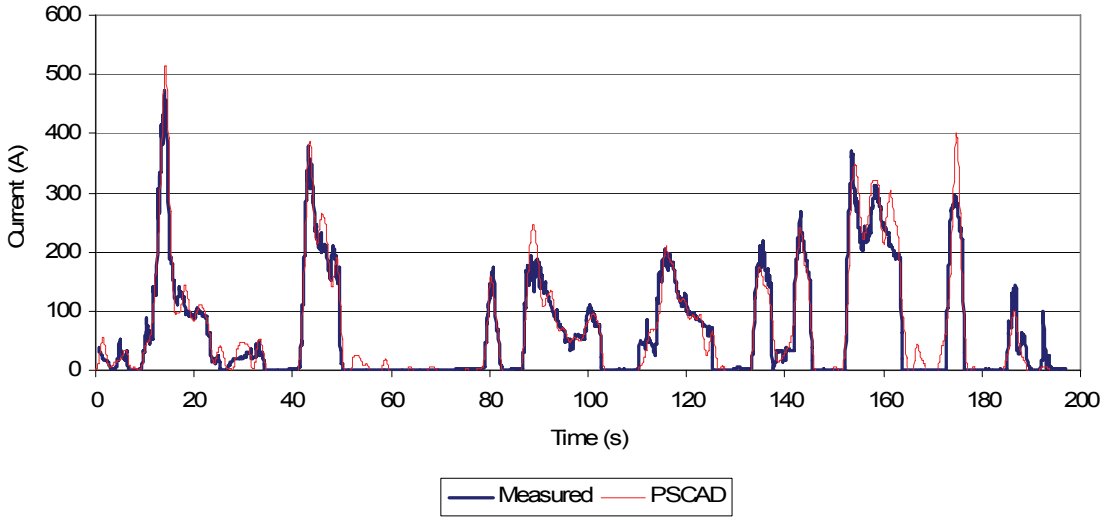

Figure 6.5 - Battery current from prototype and simulation model

Since the prototype vehicle does not currently have regenerative braking capability, this option is disabled for the simulation model. As can be seen from these tests, the battery voltage drops much more during hard accelerations in the simulation as compared to the prototype. This also leads to some differences in magnitude for the battery current in Figure 6.5. This is because the battery model parameters in the simulation were not adjusted to match the real batteries; rather they were simply taken from the literature. The total power and battery amp-hours consumed during this trial are summarized in Table 6.1.

Table 6.1 - Comparison of prototype and simulation results

Parameter	Prototype	Simulation	Difference
Distance Traveled (km)	1.343	1.343	0 %
Battery Amp-hours Consumed (Ah)	3.559	3.756	5.54 %
Battery Energy Consumed (kWh)	0.2401	0.2522	5.04 %

As can be seen, the simulation is able to predict the approximate power requirements when exposed to a given driving cycle. Additionally, the general form of

the voltage and current from the battery has been predicted as well, but there are a few notable differences.

Firstly, we do not expect the curves from the simulation to match the prototype values exactly in any case, since we are relying on a PI controller to decide how much acceleration is required to follow the same course as the real driver. Various uncontrollable factors such as changes in the road conditions, bumps, and wind gusts are obviously ignored. In fact, the very last current pulse in Figure 6.5 differs from the simulation model because of a small hill.

Finally, the values for the parameters of the battery simulation model are obviously inaccurate. The general form of the voltage resembles what is happening with the prototype, but the magnitudes of the voltage drops are too steep. This issue will be worked on in the following section.

6.5 Battery Parameter Optimization

In order to make the voltage response of the simulated battery more similar to the Optima D35 batteries of the prototype vehicle, the voltage and current data obtained from the prototype vehicle will be used to optimize the model parameters. Simplex optimization is used in a similar fashion as in section 4.3, where parameters are adjusted to minimize accumulated error over a recorded cycle. The circuit parameters, the resistances and capacitances used to model the voltage response of the battery are adjusted by the Simplex optimization routine using variable circuit elements as shown in Figure 6.6. This model is explained in section 4.2.4.

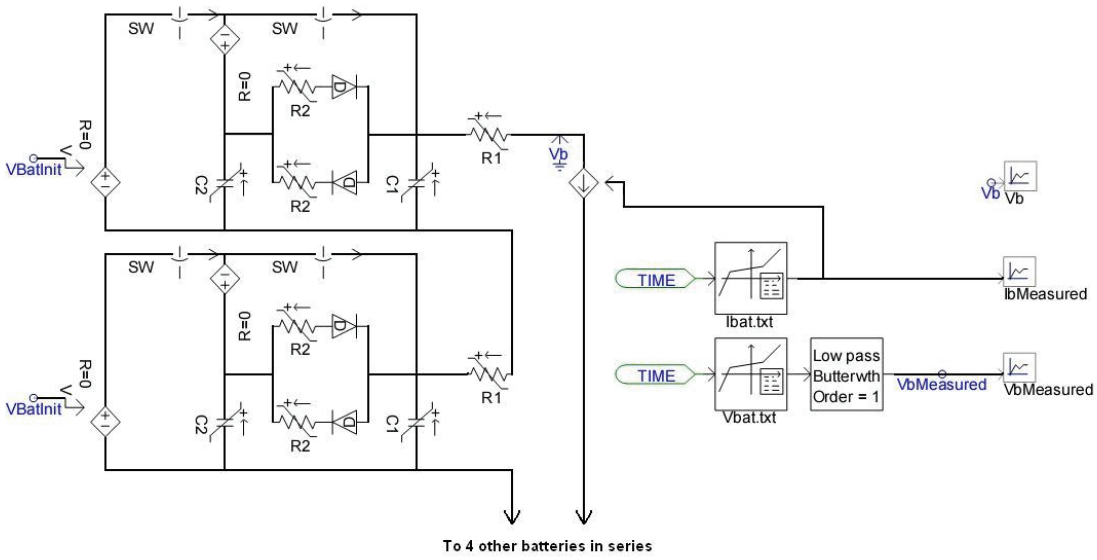

Figure 6.6 - Battery parameter optimization circuit

The current and voltage data recorded from the prototype vehicle are stored in the PSCAD input file format as Ibat.txt and Vbat.txt. The resistance R2 is used as an easy way to modify the on-resistance of the diode. The real current from the test is drawn from the battery bank by using an ideal current source, and the simulated voltage is compared against the voltage from the prototype. As the variable circuit element values are changed by the optimization routine, the simulated voltage response will gradually become closer to that of the prototype. The objective function used for the optimization is written in equation 6.1, and the connections to the simplex block are shown schematically in Figure 6.7.

$$O = \int \left(\frac{Vb_{Simulated} - Vb_{Measured}}{100} \right)^2 \cdot dt \qquad (6.1)$$

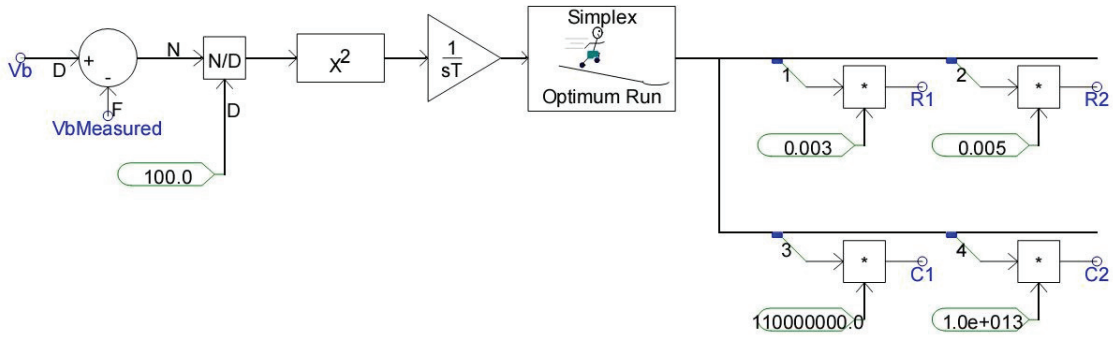

Figure 6.7 - Battery optimization objective function and simplex output

This simulation case can be run at much larger solution time steps than for the basic case, which speeds the optimization process considerably. This is because there is no power electronic switching contained in this simulation, and the time constants involved in battery modeling are reasonably long. A time step of 1ms was used here, which allowed this simple case to run much faster than real-time. After 99 runs, the tolerance is reached and the optimization is complete. The results of this optimization are given in Table 6.2.

Table 6.2 - Battery parameter optimization summary

Parameter	Before Optimization	After Optimization
R1	0.003 Ω	0.00151 Ω
R2	0.005 Ω	0.00617 Ω
C1	110 F	177.6 F
C2	$10x10^6$ F	$1.21x10^7$ F
Objective Function Result	43.507	36.897

6.6 Simulation Verification with Optimized Battery Parameters

Now that the parameters of the battery have been adjusted to better approximate the response seen from the prototype test drive in section 6.4, the simulation verification

is retried in the hopes that the resulting curves will be a closer match. The results of this trial are shown in the following figures.

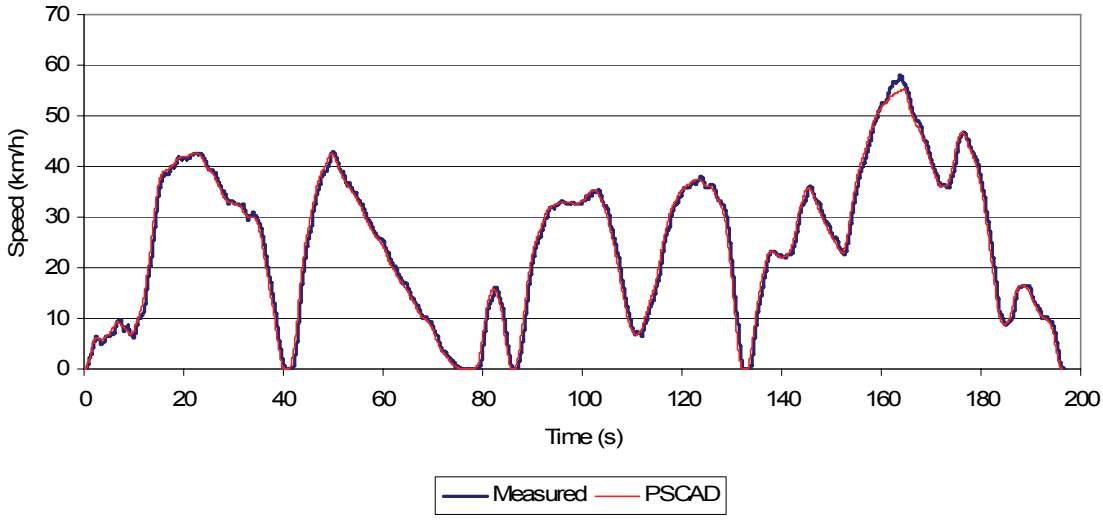

Figure 6.8 - Comparison of simulated and measured vehicle speeds

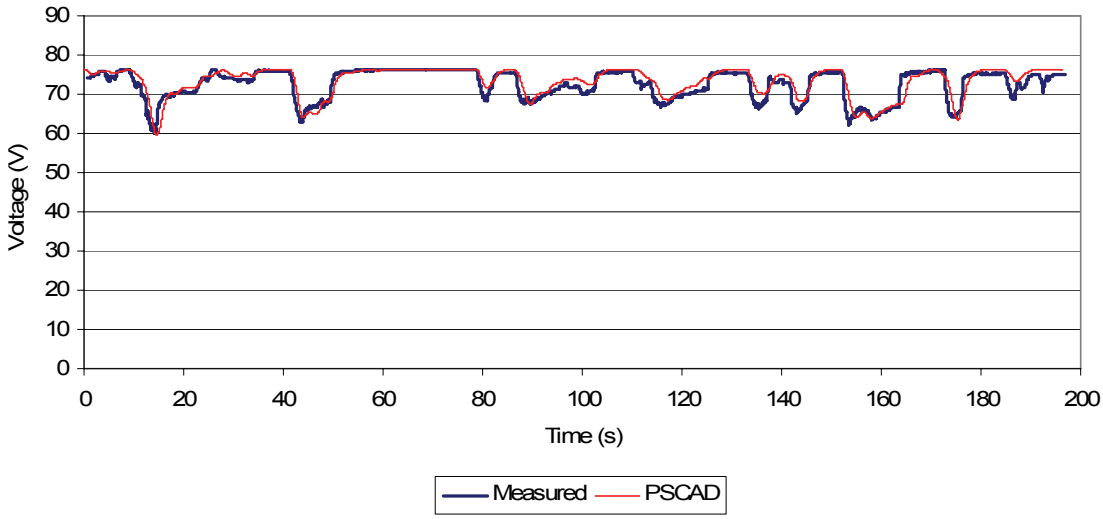

Figure 6.9 - Comparison of simulated and measured battery voltage

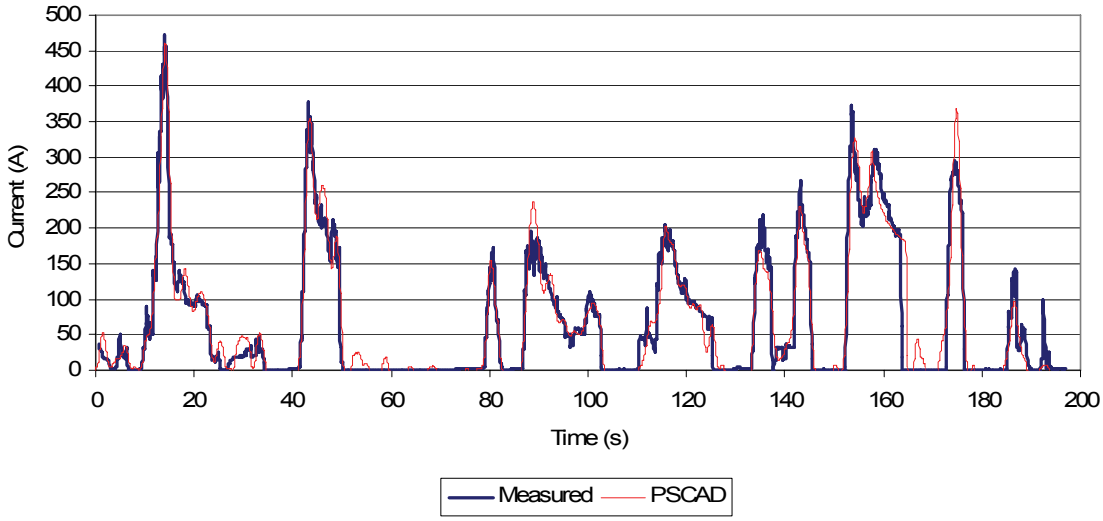

Figure 6.10 - Comparison of simulated and measured battery current

As can be seen from Figure 6.8, the simulation model is now unable to follow the prototype vehicle in its high speed acceleration near 160s. It is also interesting to note that the previous battery parameters allowed the simulation to follow the prototype completely. Figure 6.10 suggests that in this case, both the prototype and the simulation model have reached a limit in their acceleration capability, the occurrence of which is dependant on the battery response, among other things (See section 4.4). It is anticipated that the simulation model and the prototype are operating very close to the same way during this time, except that the maximum acceleration capability for the simulation model is slightly less than for the prototype vehicle. This could be a consequence of changes in the road conditions as well. As a result of this problem the simulated and prototype vehicle will travel slightly different distances over this test, the amount of which is given by the integral of the enclosed area between the curves.

Despite this interesting occurrence mentioned above, the battery voltage and current show a promising amount of correlation after the battery parameter optimization

procedure has been followed. The power requirements from the simulation and the prototype are compared in Table 6.3.

Table 6.3 - Comparison of simulated and prototype power requirements

Parameter	Prototype	Simulation	Difference
Distance Traveled (km)	1.343	1.340	-0.22 %
Battery Amp-hours Consumed (Ah)	3.559	3.642	2.33 %
Battery Energy Consumed (kWh)	0.2401	0.2505	4.33 %

The power consumption numbers shown in Table 6.3 indicate that some improvement has been seen in the accuracy of the energy consumption as well. Although the largest contributor to this energy consumption will be dictated by the accuracy of the coastdown test numbers, the role of the series resistance of the battery has a direct effect on the energy efficiency.

6.6.1 Battery Modeling Considerations

It should be noted that the insight gained by the use of the Amp-hours consumed data as shown in Table 6.3 has little meaning when comparing this strictly against the Amp-hour capacity of the batteries. This is because the series resistance within the battery model reduces the efficiency of the battery as the delivered current increases. The Amp-hour rating of these batteries (Optima D35 - 48Ah) means we would expect the battery to last 20 hours delivering 2.4 A. This is known as the C/20 capacity, which is widely used for lead-acid batteries. Additionally, it is widely understood that the parameters of the battery model will change depending on the state of charge of the battery, which raises the complication of predicting the total energy capacity of traction batteries for a given drive cycle.

However since this is to be a hybrid vehicle, with an engine used to maintain the batteries near a predetermined state of charge, these battery modeling complications are

not so important. Using a battery model such as this which has been tuned to be reasonably accurate within the window of operation should suffice. Improved battery models that can predict the conditions of the battery throughout a wider state of charge window would be important for simulating an all-electric vehicle.

6.7 Drive Cycle Testing with Optimized Battery Parameters

In Chapter 4, the New York City Cycle Driving Schedule (NYCCDS) was used to predict the energy efficiency of the hybrid vehicle during its use for parking patrol. A rough estimate of the translation of this efficiency into the domain of miles per gallon (mpg) equivalency was also done to allow comparison with the gasoline vehicle. Now that a prototype vehicle has been built and used to verify the simulation model against, the results of these tests could change. A comparison of the NYCCDS efficiency is again evaluated with and without regenerative braking by simulation, as shown in the following figures.

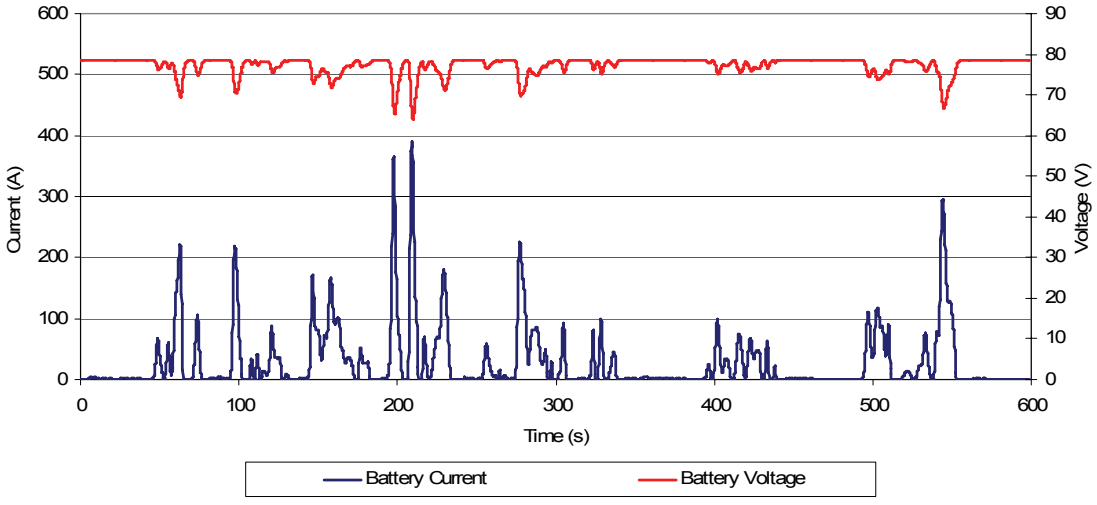

Figure 6.11 - NYCCDS battery current and voltage without regenerative braking

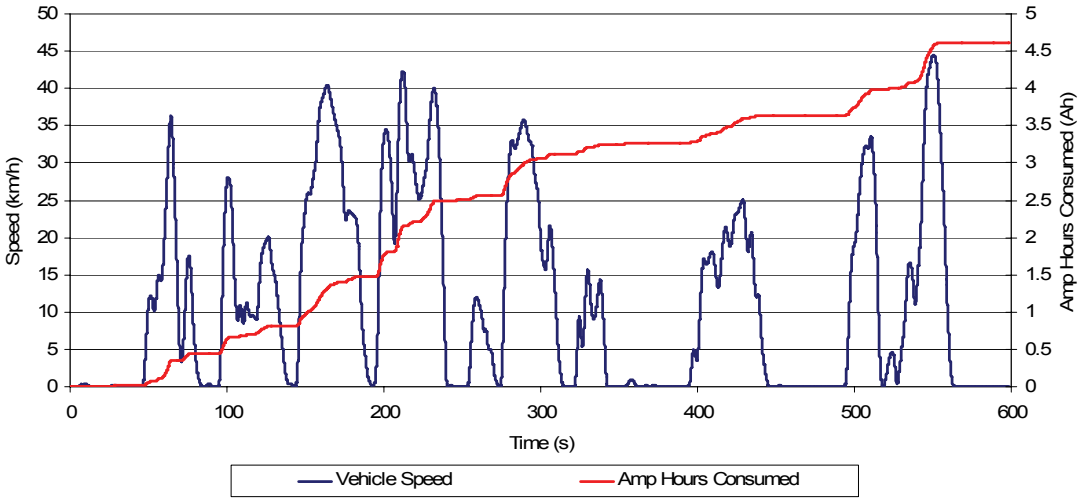

Figure 6.12 - NYCCDS vehicle speed and amp-hours without regenerative braking

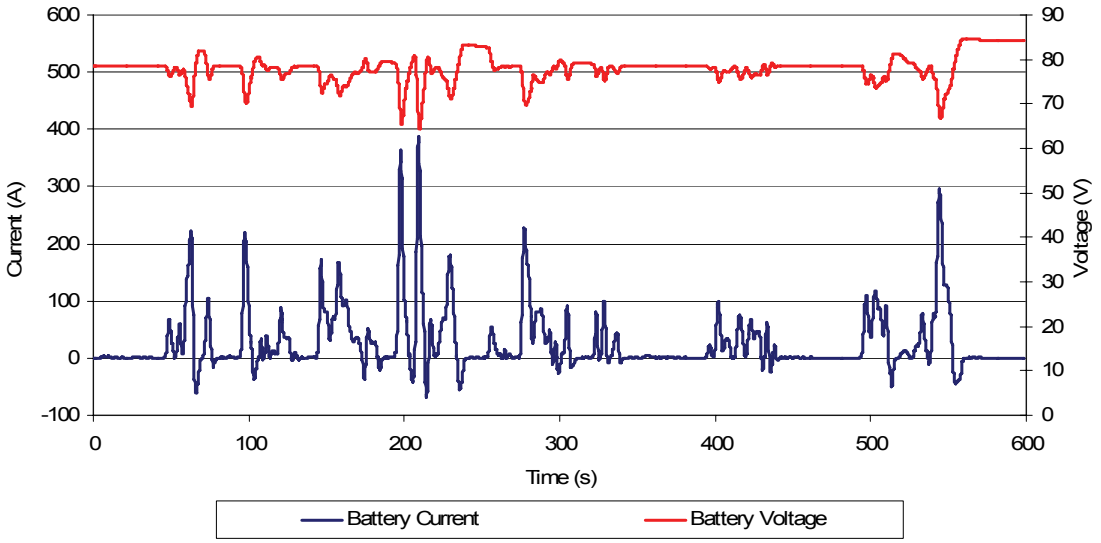

Figure 6.13 - NYCCDS battery current and voltage with regenerative braking

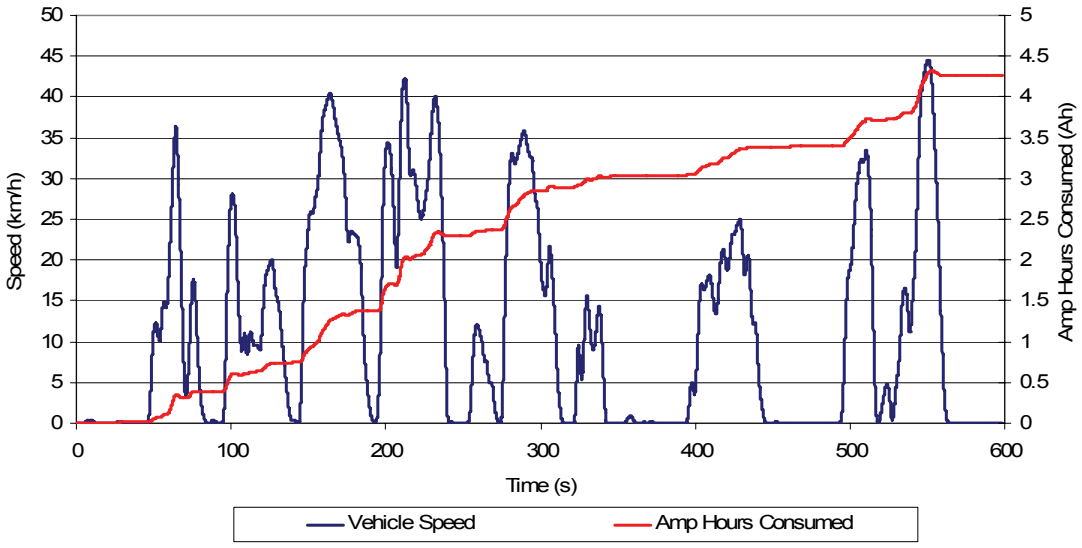

Figure 6.14 - NYCCDS vehicle speed and amp-hours with regenerative braking

Table 6.4 - NYCCDS simulation results with new parameters

Parameter	No Regenerative Braking	Regenerative Braking	Percent Improvement
Distance	1.8988 km		
kWh	0.3383	0.3120	8.43%
Ah	4.607	4.270	7.89%
Estimated mpg	28.62	31.04	8.46%

As can be seen from the simulation results above, regenerative braking provides a diminished but still significant advantage in terms of energy efficiency, and is an important benefit that an electric drive system can provide. Since the rolling and aerodynamic drag coefficients are significantly larger for the prototype, much more power has been lost due to drag forces, increasing the total required energy.

Note that the increased rolling drag for the prototype should be expected, since the PMDC machine windage and friction, as well as energy loss in the planetary gearboxes are now part of this constant. The humidity and temperature of the air also can affect the results of a coastdown test. The reason for the less favorable improvement for

regenerative braking is mainly because it is being divided by the greater total energy consumption for the trial. The amp-hours consumed from the battery pack, 4.27 Ah for the regenerative case, is an informative figure for evaluating the capacity of the battery pack. It is important to note however that the actual proportion of capacity lost from the battery during this test depends on the rate at which it was withdrawn. Considering this, 48 Ah batteries would not last very long in this case without the use of the engine. The mpg estimations in Table 6.4 follow the same analysis given in Chapter 4.

Although the results are not as good as predicted in Chapter 4, they are still expected to be much better than for the gasoline model exposed to such an erratic driving profile. However it is clear that any mechanical design improvements that could improve the coastdown parameters would be quite beneficial. In fact, an effort is already underway during the time of this writing to streamline the aerodynamic design of the vehicle.

7 CONCLUSIONS AND RECOMMENDATIONS

7.1 Contributions

A series hybrid electric drivetrain, with the exclusion of the engine and generator unit, has been designed for the specialty application of parking patrol. The design process included the development of an electromagnetic transient simulation model in PSCAD/EMTDC, which is capable of modeling the electrical, mechanical, and control systems in high detail.

1. Electric motors, power electronic drives, and lead-acid batteries were selected for the vehicle based on preliminary design calculations and the availability of other important system components. Cost, weight, volume, and longevity were important factors affecting this process.
2. These components were modeled with PSCAD/EMTDC using a combination of standard library components and custom developed blocks. The parameters of these simulation components were selected based on equipment specifications and physical measurements of the vehicle.
3. The design was then evaluated against various performance indices and a prediction of the fuel economy for the final design was made.

A physical prototype of the hybrid electric drivetrain, without the engine and generator set, was built to the specifications obtained from the simulation model. Several advanced hardware and software features were developed to make this prototype a convenient test bed for the evaluation of the design.

1. A custom embedded microcontroller system was designed and built to perform various control and monitoring functions. The vehicle was fitted with current and voltage sensors to measure the response at the battery terminals. Wheel speed sensors are used to determine the speed of the vehicle.
2. Data from a test trial was logged and analyzed to determine various physical parameters of the prototype vehicle.
3. Prototype data was used to optimize the simulation model parameters for the battery bank, thus improving the agreement between the simulation and prototype response considerably.
4. The verified and reconciled simulation model was used to make better predictions of fuel economy for the prototype vehicle under usage conditions similar to its intended use of parking patrol. Benefits of regenerative braking were also examined.

7.2 Recommendations

Although the simulation model and prototype have been used to great benefit for the analysis of the hybrid drivetrain for this application, there remain many opportunities to improve this strategy in the future.

1. The battery model could be improved significantly. Experimentation and consultation with the literature have shown that the parameters used for the battery model are only valid for a certain state of charge and state of health of the battery. Increasing the detail and complexity of the model could be done to account for these changes.

2. Although strictly not necessary for academic investigations into battery-based hybrid drivetrain design, an investigation into the longevity of the battery bank while exposed to different charge and discharge profiles would be of great interest to industry. The ability to model complex battery management systems would also be an asset.
3. The addition of accurate engine modeling capability and the development of an energy management scheme are natural next steps in this development. The engine model would be able to predict the amount of fuel and emissions that are released during its operation. An energy management scheme could then be developed to benefit the fuel consumption and emissions of the engine, as well as the longevity and reliability of the battery bank.
4. The ability to model internal combustion engines for fuel and emissions using this simulation environment would allow for this design process to be extended to parallel and other hybrid configurations.

In summary, a significant first step in the development of hybrid electric vehicle modeling capability within PSCAD/EMTDC has been developed. This simulation has been verified against a prototype vehicle with reasonable accuracy. The simulation has been used effectively as a design tool to reduce the amount of time and money spent during the prototype stage. An investigation of the feasibility of the series hybrid electric drivetrain for application to the parking patrol market has taken place and shown some definite promise.

REFERENCES

[1] D. Stevens, *"Petrol and Diesel are Dead – Says GM," Autocar,* June 11, 2007. [Online] Available: http://www.autocar.co.uk/News/NewsArticle/AllCars/225989. [Accessed: June 15, 2007].

[2] R. von Helmolt, U. Eberle, "Fuel cell vehicles: Status 2007," *Journal of Power Sources*, vol. 165, no. 2, pp. 833-843, January 2007. [Online] Available: http://www.sciencedirect.com/science/article/B6TH1-4MTC6HN-2/2/e75d4f21be5f46da23920b01083f728f [Accessed: May 28, 2007].

[3] P. Van den Bossche, F. Vergels, J. Van Mierlo, J. Matheys, W. Van Autenboer, *"SUBAT: An assessment of sustainable battery technology," Journal of Power Sources*, vol. 162, no. 2, pp. 913-919, November 2006. [Online] Available: http://www.sciencedirect.com/science/article/B6TH1-4GXVG7C-3/2/765a308efb8ff98b2b3a7ebab9ce13db. [Accessed: May 28, 2007].

[4] M.C. Trummel, A.F. Burke, "Development History of the Hybrid Test Vehicle," in *IEEE Transactions on Vehicular Technology*, vol. 32, no. 1, pp. 7-14, February 1983.

[5] F.Z. Peng, M. Shen, K. Holland, "Application of Z-Source Inverter for Traction Drive of Fuel Cell-Battery Hybrid Electric Vehicles," in *IEEE Transactions on Power Electronics*, vol. 22, no. 3, pp. 1054-1061, May 2007.

[6] L.O. Hewko, T.R. Weber, "Hydraulic Energy Storage Based Hybrid Propulsion System For A Terrestrial Vehicle," in *Proceedings of the 25th Intersociety Energy Conversion Engineering Conference,* Reno, Nevada, vol. 4, pp. 99-105, August 1990.

[7] I.J. Albert, E. Kahrimanovic, A. Emadi, "Diesel sport utility vehicles with hybrid electric drive trains," in *IEEE Transactions on Vehicular Technology*, vol. 53, no. 4, pp. 1247-1256, July 2004.

[8] N. Jalil, N.A. Kheir, and M. Salman, "A rule-based energy management strategy for a series hybrid vehicle," in *Proceedings of the American Control Conference*, Albuquerque, New Mexico, pp. 689-693, 1997.

[9] J. Voelcker, "Top 10 Tech Cars," *IEEE Spectrum*, vol. 44, no. 4, pp. 34-41, April 2007.

[10] A. Emadi, K. Rajashekara, S. S. Williamson, and S. M. Lukic, "Topological overview of hybrid electric and fuel cell vehicular power system architectures and configurations," *IEEE Transactions on Vehicular Technology*, vol. 54, no. 3, pp. 763-770, May 2005.

[11] General Motors Corporation, *"Saturn VUE Green Line Hybrid," General Motors Corporation,* 2006. [Online] Available: http://www.gm.com/company/gmability /adv_tech/100_news/hybridvue2_10906.html. [Accessed: March 9, 2006].

[12] Ford Motor Company, "Ford Escape Hybrid," Ford Motor Company, 2007. [Online] Available: www.fordvehicles.com/escapehybrid. [Accessed: May 20, 2007].

[13] American Honda Motor Company, *"2007 Honda Accord Hybrid – Technology," American Honda Motor Company,* 2007. [Online] Available: http://automobiles.honda.com/models/accord_hybrid.asp?ModelName= Accord+Hybrid&function=technology. [Accessed: February 17, 2007].

[14] Toyota Motor Corporation *"Hybrid Synergy Drive," Toyota Motor Corporation,* 2007. [Online] Available: www.hybridsynergydrive.com. [Accessed: February 17, 2007].

[15] US Department of Transportation – National Highway Traffic Safety Administration, *"Federal Motor Vehicle Safety Standards - 571.305 - Electric-powered vehicles: electrolyte spillage and electrical shock protection,"* US Department of Transportation, 2003.

[16] J.M. Miller, *Propulsion Systems for Hybrid Vehicles,* IEE Power and Energy Series. London: Institution of Electrical Engineers, 2004.

[17] J.B. Heywood, *Internal Combustion Engine Fundamentals*. New York: McGraw-Hill, 1988.

[18] N. Kamenev, E. Dirks, *GO-4 Interceptor II Coastdown Data,* [email] March 3, 2006.

[19] Robert Bosch GmbH, Bosch Automotive Handbook, 6th Edition, Robert Bosch GmbH, 2004.

[20] N.K. Medora, A. Kusko, "Dynamic Battery Modeling of Lead-Acid Batteries using Manufacturers' Data," in *Proceedings of the 27th International Telecommunications Conference*, Berlin, pp. 227-232, September 2005.

[21] Enigma Industries, "*PMG 132," Enigma Industries,* 2006. [Online]. Available: http://www.enigmaindustries.com/PMG_132/PMG_132.htm. [Accessed: May 23, 2007].

[22] DMC GmbH, *Pro Controller Manual,* rev. 3.02, DMC GmbH, 2006.

[23] International Rectifier, *HV floating MOS-gate driver ICs,* Application Note AN-978.

[24] US Environmental Protection Agency, *"Dynamometer Driver's Aid" US Environmental Protection Agency,* 2007. [Online] Available: http://www.epa.gov/nvfel/testing/dynamometer.htm. [Accessed: February 12, 2007].

ADDITIONAL RESOURCES

[1] A. Di Napoli, F. Crescimbini, L. Solero, F. Caricchi, F. G. Capponi, "Multiple-input DC-DC Power Converter for Power-Flow Management in Hybrid Vehicles," in *Proceedings of the Industry Applications Conference,* Pittsburgh, Pennsylvania, vol. 3, no. 1, pp. 1578-1585, October 2002.

[2] L. Solero, A. Lidozzi, J.A. Pomilio, "Design of Multiple-Input Power Converter for Hybrid Vehicles," in *IEEE Transactions on Power Electronics,* vol. 20, no. 5, pp. 1007-1016, September 2005.

[3] J.B. Olson, E.D. Sexton, "Operation of Lead-Acid Batteries for HEV Applications," in *Proceedings of the Battery Conference on Applications and Advances,* Long Beach, California, vol. 1, no. 1, pp. 205-210, January 2000.

[4] H. Shimizu, J. Harada, C. Bland, K. Kawakami, L. Chan, "Advanced Concepts in Electric Vehicle Design," in *IEEE Transactions on Industrial Electronics,* vol. 44, no. 1, pp. 14-18, February 1997.

[5] L. Zubieta, R. Bonert, "Design of a Propulsion System With Double-Layer Power Capacitors for a Hybrid-Electric Automobile," in *Proceedings of the 2003 Electric Vehicle Symposium,* Long Beach, California, November 2003.

[6] M. Ceraolo, P. Capozzella, F. Baronti, "CAN-LabView based Development Platform for fine-tuning Hybrid Vehicle Management Systems," in *Proceedings of the Vehicle Power and Propulsion Conference,* Chicago, Illinois, pp. 433-438, September 2005.

[7] M. R. Cuddy and K. B. Wipke, "Analysis of the fuel economy benefit of drivetrain hybridization," in *SAE Technical Paper Series,* no. 970289, February 1997.

[8] R. Schupbach, J.C. Balda, M. Zolot, and B. Kramer, "Design methodology of a combined battery-ultracapacitor energy storage unit for vehicle power management," in *Proceedings of the IEEE Power Electronics Specialist Conference,* Acapulco, Mexico, vol. 1, no. 1, pp. 88-93, June 2003.

[9] M. Chen, G.A. Rincon-Mora, "Accurate Electrical Battery Model Capable of Predicting Runtime and I–V Performance," in *IEEE Transactions on Energy Conversion,* vol. 21, no. 2, pp. 504-511, June 2006.

[10] S.S. Williamson, S.M. Lukic, A. Emadi, "Comprehensive Drive Train Efficiency Analysis of Hybrid Electric and Fuel Cell Vehicles Based on Motor-Controller Efficiency Modeling," in *IEEE Transactions on Power Electronics,* vol. 21, no. 3, pp. 730-740, May 2005.

[11] O. Bohlen, S. Buller, R.W. De Doncker, M. Gelbke, R. Naumann, "Impedance Based Battery Diagnosis for Automotive Applications," in *Proceedings of the IEEE Power Electronics Specialists Conference,* Aachen. Germany, vol. 4, no. 1, pp. 2792-2797, June 2004.

[12] N. Medora, A. Kusko, "An Enhanced Dynamic Battery Model of Lead-Acid Batteries Using Manufacturers' Data," in *Proceedings of the International Telecommunications Energy Conference,* Providence, Rhode Island, pp. 1-8, September 2006.

[13] A.F. Burke, "Batteries and Ultracapacitors for Electric, Hybrid, and Fuel Cell Vehicles," in *Proceedings of the IEEE,* vol. 95, no. 4, pp. 806-820, April 2007.

[14] Y. Hyunjae, S. Seung-Ki; P. Yongho, J. Jongchan, "System Integration and Power Flow Management for a Series Hybrid Electric Vehicle using Super-capacitors and Batteries," in *Proceedings of the IEEE Applied Power Electronics Conference,* Anaheim, California, pp. 1032-1037, February 2007.

[15] Z.M. Salameh, M.A. Casacca, W.A. Lynch, "A Mathematical Model for Lead-Acid Batteries," in *IEEE Transactions on Energy Conversion,* vol. 7, no. 1, pp. 93-98, March 1992.

[16] P.E. Pascoe, A.H. Anbuky, "VRLA Battery Discharge Reserve Time Estimation," in *IEEE Transactions on Power Electronics,* vol. 19, no. 6, pp. 1515-1522, November 2004.

[17] P.T. Krein, R.S. Balog, "Life extension through charge equalization of lead-acid batteries," in *Proceedings of the International Telecommunications Energy Conference,* Montreal, Quebec, pp. 516-523, September 2002.

[18] J.Y. Wong, *Theory of Ground Vehicles,* 3rd ed. New York: John Wiley, 2001.